Deep–Sea Research II 173 (2020) 104763

Contents lists available at ScienceDirect

Deep-Sea Research Part II

journal homepage: http://www.elsevier.com/locate/dsr2

Temporally-resolved mechanisms of deep-ocean particle flux and impact on the seafloor carbon cycle in the northeast Pacific

Christine L. Huffard [a,*], Colleen A. Durkin [b], Stephanie E. Wilson [c], Paul R. McGill [a], Rich Henthorn [a], Kenneth L. Smith Jr. [a]

[a] Monterey Bay Aquarium Research Institute, Moss Landing, CA, USA
[b] Moss Landing Marine Laboratories, Moss Landing, CA, USA
[c] unaffiliated, United Kingdom

A B S T R A C T

High-temporal-resolution views of particle flux to the abyssal benthic boundary layer are provided for an eight-month period (October 2014–June 2015) at the long-term monitoring site Station M within the California Current ecosystem. Contributions of fecal pellets and aggregates to particulate organic carbon (POC) flux at 3900 m depth were estimated based on optical sediment trap (Sedimentation Event Sensor) images captured as a time-series of 2 h collections. POC flux estimated from Sedimentation Event Sensor (SES) images explained variation in carbon consumption and the carbon budget balance (supply – demand) with finer resolution than POC flux measurements from bulk collections by a concurrently deployed conventional sediment trap. Indicators of particle transport by benthic boundary layer currents and active transport by zooplankton were evaluated by comparing SES-estimated POC flux to measured current speed and direction, hours since solar noon, and modeled lunar illumination at the surface. Influence of particles (fecal pellets and aggregates) on the carbon budget was evaluated by comparing particle-specific contributions to POC flux with sediment community oxygen consumption (SCOC) measured by the Benthic Rover at 4000 m depth. During the eight-month sampling period, salp fecal pellets delivered an estimated 45% of the total POC flux to the benthic boundary layer and were responsible for an estimated 74% of a temporary carbon surplus in May and June 2015. Salp fecal pellets also appeared to be the primary source of chlorophyll peaks at the site. By contrast, most aggregates appeared to be lower-quality particles possibly sourced from lateral advection and local rebound of recently-settled detritus, which settled according to spring-neap tidal oscillations. Some aggregates may have been fresher, as suggested by non-linear relationships with SCOC and the carbon budget balance. Results suggest sinking particles packaged in surface waters and reaching abyssal depths in fresh condition (e.g. salp fecal pellets) had a greater influence on carbon consumption (e.g. SCOC) and the carbon budget balance than more refractory particles.

1. Introduction

Improving carbon budgets through full-ocean depths requires a better understanding of the mechanisms driving particle production, vertical transport, and consumption (Christina and Passow, 2007; Estapa et al., 2017; Boyd et al., 2019; Stukel et al., 2017). Ecological processes transform surface-derived carbon into particles, such as fecal pellets and aggregates, which have different sinking speeds and trophic qualities (Cavan et al., 2015; Turner, 2015; Wilson et al., 2008). They are transported downward through the water column by a variety of physical and biological mechanisms, which strongly influence the depth and rates at which carbon is consumed (Boyd et al., 2019). A highly variable amount of carbon in these particles reaches the deep sea, where it may be sequestered from the atmosphere for hundreds to thousands of years (Boyd et al., 2019). Most of this carbon is consumed by food-limited seafloor communities (Ruhl, 2008; Smith et al., 2014); the small fraction that evades this consumption may be sequestered in sediments for millennia (Dickens et al., 2004). Improving biogeochemical models will require identifying the particles responsible for carbon flux to the deep sea, understanding their vertical transport mechanisms (Le Moigne, 2019), and measuring their impact on the seafloor carbon budget at high temporal resolution.

A particle's origin and processing strongly influence its impact on deep-sea carbon budgets. Particles that package surface production and transport it rapidly below the mixed layer, such as larvacean houses (Robison et al., 2005), and krill fecal pellets (Gleiber et al., 2012; Belcher et al., 2019), deliver a significant quantity of carbon to the deep sea (Guidi et al., 2009; Riley et al., 2012). This material provides a high-quality food resource to seafloor communities, which begin consuming it almost immediately after it settles (Witte et al., 2003; Smith et al., 2014). By contrast, particles formed deeper in the water column, from more refractory material, are less carbon-rich (Ransom et al., 1998) but they hasten the downward flux of particles that might have remained suspended otherwise (e.g. Wilson et al., 2008). Vertical

* Corresponding author.
E-mail address: chuffard@mbari.org (C.L. Huffard).

https://doi.org/10.1016/j.dsr2.2020.104763
Received 29 June 2019; Received in revised form 15 January 2020; Accepted 19 February 2020
Available online 21 February 2020

migrations and coprophagy by zooplankton may be particularly important to repackaging and export mechanisms, as evidenced by variation in the relative abundance of different particle types with depth and over time (Vinogradov and Evgen'evich, 1970; Urrère and Knauer, 1981; Miquel et al., 2015; Belcher et al., 2017). Packaging depth, and carbon quality and content, are not known for all particle types. For example, the term "aggregate" applies to fresh, carbon-rich phytodetrital material that can sink rapidly from the surface to the sea floor (Thiel et al., 1989), or it can apply to marine snow packaged deep in the water column and comprised of heavily processed material (Alldredge, 1998). In the benthic boundary layer, aggregates can represent detritus that settled briefly but was "rebounded" by currents back into the water column before incorporating into sediments (Walsh et al., 1988; Beaulieu and Baldwin, 1998). Aggregates that form in the nepheloid layer from resuspended sediments (Turnewitsch et al., 2017) by benthic storm activity or lateral advection (Beaulieu and Baldwin, 1998) have considerably higher clay content and lower organic carbon content than fresh surface-derived material (Ransom et al., 1998). Most fecal pellets sampled at abyssal depths are assumed to be repackaged multiple times (Wilson et al., 2008; Shatova et al., 2012; Conte et al., 2001). However, the ubiquitous presence of unexpectedly fresh surface-derived particles in the deep sea (Agusti et al., 2015), considerable variation in sinking speeds of fecal pellets (Svensen et al., 2012; Liszka et al., 2019), and the importance of short-term (days to weeks), high-magnitude deposition events to annual deep-sea carbon budgets (Smith et al., 2018) calls for a more detailed understanding of particle sources.

In addition, the mechanisms by which particles are transported downward through the water column affect their role in global carbon export. Gravitational sinking of particles is estimated to account for 60% of carbon transport in the oceans, but most of this carbon is estimated to stay in the upper 250 m (Boyd et al., 2019). The remaining 40% of transport is associated with physical or biological pathways—"particle injection pumps"—by which carbon may enter deeper waters (Boyd et al., 2019). Subduction and active transport by vertical migrators are examples of particle injection pumps. While their contributions to carbon budgets are typically tallied separately, these mechanisms can work in concert. Subduction can significantly enhance gravitational sinking (Stukel et al., 2017). Vertical migrators that deposit large, fast-sinking fecal pellets into the mesopelagic (such as salps; Wiebe et al., 1979; Iversen et al., 2017) contribute to both active transport and gravitational sinking. Studies are needed to resolve and synthesize these carbon export pathways below the mesopelagic, so that predictive biogeochemical models can be improved (Le Moigne, 2019).

Many physical and biological mechanisms governing gravitational sinking and particle injection are known to cycle predictably over time, even if the exact onset of single influential events (such as storms or phytoplankton blooms) cannot be foreseen. Incorporating temporal patterns into global climate models can improve ocean carbon cycle forecasts (Lutz et al., 2007). The mixed layer is generally deepest in the winter (e.g. Steinberg et al., 2001), which seasonally enhances large-scale physical pumping mechanisms (Boyd et al., 2019). Fed by surface processes, abyssal habitats experience seasonal peaks in carbon supply (Lampitt et al., 2010; Baldwin et al., 1998; Wong et al., 1999), demand (Witbaard et al., 2000; Smith et al., 2016), and possibly carbon storage in the sediments (e.g. Danovaro et al., 2001). Phytoplankton production (Harding et al., 1987) and diel vertical migrations by zooplankton (Isla et al., 2015) cycle seasonally, but also at daily and monthly scales along with changes in solar and lunar illumination (Cisewski et al., 2010; Ochoa et al., 2013; Last et al., 2016). Trophic interactions may drive depth-tiered diel vertical migrations that extend into the bathypelagic, where surface illumination is not detectable above ambient bioluminescence (Ochoa et al., 2013). Tidal fluid dynamics are important drivers of carbon export near seamounts (e.g. Turnewitsch et al., 2016), and studies of deep-sea biogeochemistry may find tidal cycles to be important drivers of carbon processing (Turnewitsch et al., 2017). For example, at the Porcupine Abyssal Plain, the neap-spring tidal transition appears to increase aggregation of material in the benthic boundary layer and reduce deposition of aggregates onto the sea floor (Turnewitsch et al., 2017). At a finer temporal scale, semidiurnal tides can be associated with increased turbidity near the sea floor (Vangriesheim et al., 2001; Turnewitsch et al., 2017), and vertical movements of abundant benthopelagic zooplankton (Smith et al., 2020).

Particles with very different sources and transport histories may be differentiated by the temporal variability of their downward flux. Particles packaged in surface waters may settle at rates that retain temporal cycles linked to surface drivers of production and vertical migration, including solar and lunar illumination. By contrast, particles packaged in the benthic boundary layer may settle in cycles corresponding with tidal currents near the sea floor. Patterns of flux in relation to ambient currents may further differentiate local resuspension from lateral advection. Regardless of particle type, those packaged in surface waters and transported downward in fresh condition may have higher carbon content, fuel greater carbon consumption, and lead to greater carbon surpluses in the deep sea compared to more refractory particles, such as those packaged at greater depths.

To work toward a mechanistic understanding of carbon cycling in the deep sea, we present high-temporal resolution views of particle flux, transport, and carbon demand at the long-term abyssal monitoring site Station M. This site experiences seasonal and interannual changes in carbon supply in relation to surface conditions and climate (Smith and Druffel, 1998), as well as lateral advection of resuspended material in the benthic boundary layer (Beulieu and Baldwin, 1998). Overlying waters in the California Current ecosystem (CCE) exhibit high productivity (Kahru and Mitchell, 2002; Kahru et al., 2019), subduction along fronts (Stukel et al., 2017), and vertical migrations by zooplankton (Ohman and Romagnan, 2016). These attributes make it a practical system in which to discern the influences of multiple transport mechanisms on particle flux and carbon budgets. Here we provide detailed views of particle flux [quantity, type, and quality (organic carbon and phytopigment content)] at approximately 3900 m depth using the Sedimentation Event Sensor (SES; McGill et al., 2016). Next, indicators of particle transport by currents and active transport by vertically migrating zooplankton were evaluated by comparing SES-estimated POC flux to i) current speed and direction measured in the benthic boundary layer, ii) hours since solar noon, and iii) modeled maximum lunar illumination at the surface. Finally, we assessed the impact of different particle types on the balance of the seafloor carbon budget (i.e. supply and demand).

2. Methods

2.1. Study location

Data are presented from instruments deployed concurrently over nearly eight months (26 October 2015–18 June 2015) in the benthic boundary layer at the long-term abyssal monitoring site Station M (~ 4000 m deep) in the CCE (Fig. 1). The quantity and quality of sinking material varies seasonally and interannually at this site (Smith et al., 2013). Fresh surface productivity occasionally reaches the sea floor (Smith et al., 2014), and resuspended sediments, presumably from upslope, reach at least 50 m above bottom (Hwang et al., 2004). Currents at the site exhibit semi-diurnal and diurnal tides (12.3 h, 25.5 h, respectively), and vary by moon phase (14 d; Smith et al., 2020) but not consistently by season (Connolly et al., 2020).

2.2. Detailed views of particle flux (quantity, type, and quality)

The quantity, type, and quality of sinking particulate matter were assessed using the SES (McGill et al., 2016) and a conventional sequencing sediment trap (McLane Parflux Mark 78H2) deployed 50 m above bottom (bottom depth 3955 m and 3964 m at SES and conventional sediment trap mooring locations respectively; Fig. 1). Both

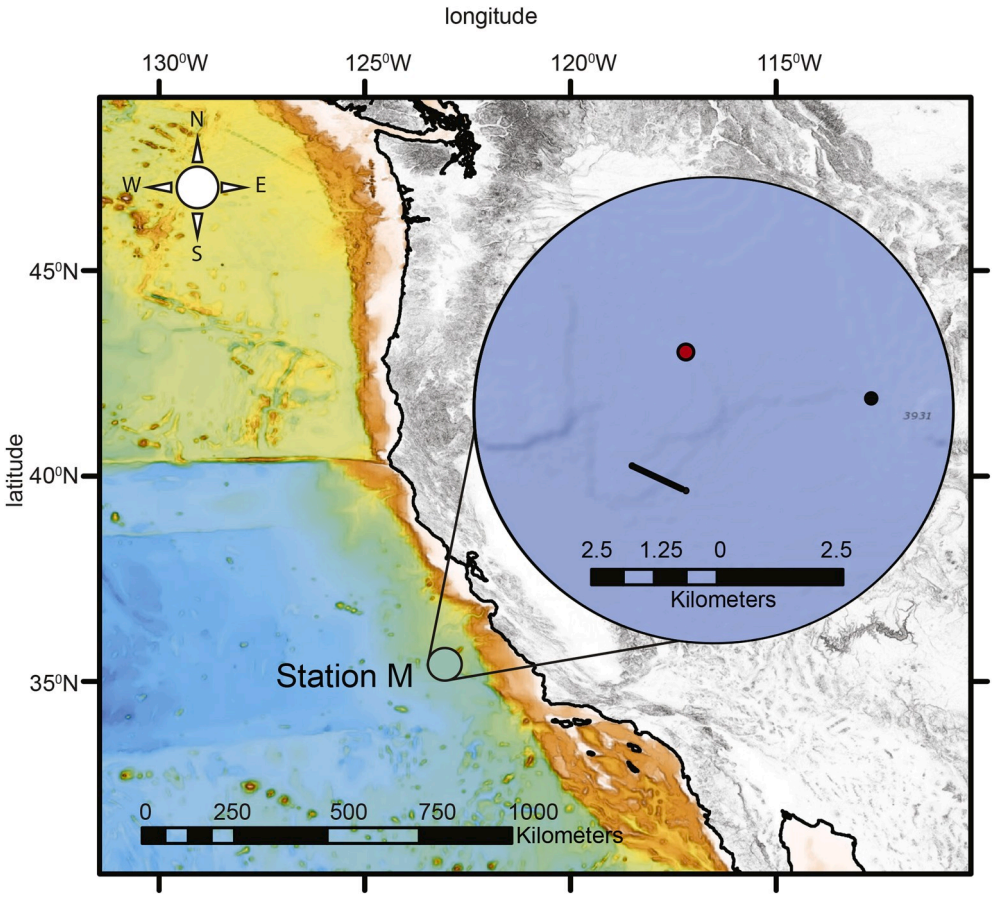

Fig. 1. Location of Station M off the California coast, with inset showing deployment locations of Sedimentation Event Sensor (35° 9.5′ N, 122° 59′ W, red dot), conventional sediment trap and time lapse camera (35° 09′ N, 122° 57′ W, black dot), and deployment (35° 8.0′ N, 122° 59.0′ W) and recovery (35° 8.27′ N, 122° 59.58′ W) locations of Benthic Rover connected by black line to approximate transect path.

instruments collected material using an upward-facing funnel with a 0.5 m^2 opening. The SES provided front- and back-lit macro images and fluorescence readings of material settling on a 25-mm diameter slide at the base of the funnel. This slide was swept clean to remove the settled material between 2-hr collection periods. A 2-h flow-through standby state separated collection periods. Individual phytoplankton cells could not be resolved by this method. The conventional sediment trap collected sinking material in a 3% formalin brine solution for subsequent laboratory analysis. Limited to 21 cups, this sediment trap had a 10 d collect period and completed its cycle 37 days before the SES deployment ended. A time-lapse camera (Smith et al., 1993) at the base of the conventional sediment trap mooring provided views of large detrital aggregates on the sea floor from 1 Nov 2014–31 May 2015. Datasets generated by these instruments are described under the sub-headings below.

2.2.1. Particle quantity: light attenuation, mass flux, and detrital aggregate seafloor cover

Three measurements of particle quantity are provided: light attenuation measured by the SES, mass flux measured by the conventional sediment trap, and coverage of detrital aggregates on the seafloor in time-lapse camera images.

Macro images taken by the SES were used to estimate light attenuation, which is considered a relative, but not necessarily linear, measure of sample opacity (McGill et al., 2016). Inverse mean pixel brightness (MPB^{-1}) of backlit images was calculated using Mathematica 10.4, and values were scaled such that an empty and a completely dark slide were set to 0% and 100% respectively. This value was used as a proxy for light attenuation. Analysis of a small empty portion of the slide confirmed no drift in brightness throughout the deployment. This portion of the slide was batch cropped from all retrieved images, and those crops that were not empty were manually removed before analyzing the mean gray value of the remainder to assess drift.

Mass flux was measured from samples collected by the conventional sequencing sediment trap. Zooplankton swimmers were removed, and a three-quarters split of each sample was freeze-dried and weighed to determine mass flux. Values were corrected for salt content using $AgNO_3$ titration (Strickland and Parsons, 1972).

Daily percent cover of detrital aggregates imaged directly on the sea floor by a time-lapse camera system (Smith et al., 1998) was assessed for qualitative comparison to fluxes collected in the conventional sequencing sediment trap on the same mooring. The time-lapse camera lens approximately 2 m above the sea floor yielded an oblique view totaling approximately 20 m^2 (Smith et al., 1993). In this view, detrital aggregates several centimeters in diameter could be resolved, but fecal pellets could not. Using the open-source software VARS (Schlining and Stout, 2006), a single observer (KLS) annotated the outline of detrital aggregates in the foreground portion of the image (approximately 9 m^2) with the optimum brightness and contrast. Horizontal lines were added in VARS to delineate a consistent field of view for annotation across all frames. Detritus was labelled as phytodetritus if it had a greenish color, and gelatinous detritus if it was white (diaphanous, filmy). Area measurements were then made in VARS, which converted screen-based annotations to areas in cm^2 based on a Canadian grid (Wakefield and Genin, 1987). These measurements were then compared to the field of view for calculation of percent cover.

2.2.2. Particle type: enumerating fecal pellets and aggregates

Particles imaged by the macro camera on the SES were detected with an image processing program created using functions available in the Python package Sci-Kit Image (van der Walt et al., 2014). All backlit images (brightfield) were converted to grayscale uint8 formatted images, including a blank image that contained no particles captured in situ. To remove the background from each brightfield image, the maximum pixel value of the blank image was subtracted from the entire blank image. This resulted in an equal shift-up of pixel intensities in the blank-difference image due to the uint8 data format. This blank-difference image was then subtracted from each sample brightfield image, also in uint8 data format. To identify potential particles, a threshold filter was applied to the background-subtracted images to select the darkest pixels. A threshold value of 170 (between 0 and 255) was chosen to identify the entire particle area with minimal background noise at the illumination intensity of this instrument. To eliminate background pixels detected by this rough thresholding approach, a Sobel filter was applied to the grayscale images to identify locations where large changes in pixel brightness occurred over a small area (i.e. edge detection). An eroded particle mask was created from the threshold image of potential particles, which was then used to mask the interior pixels of the Sobel filtered image. A brightness threshold was applied to the masked, Sobel-filtered image to identify locations with sharp gradients in pixel brightness that occurred on the outer edges of potential particles. Finally, particles were recorded if locations with in-focus edges overlapped with pixel locations of potential particles identified in the threshold image. The particle pixel surface area and bounding box coordinates were recorded and used to extract every individual particle image. Particles were manually identified and categorized as aggregates, fecal pellets, zooplankton, or unidentifiable (imaging processing noise or blurry image). Aggregates were defined as amorphous particles of detritus, and may have contained fecal pellets that could not be individually resolved. Aggregates were assumed to be composed of heterogenous material and produced by various processes, including natural aggregation of phytodetritus and other organic particles, by the degradation of fecal material, and by other zooplankton byproducts (e.g. larvacean houses). Fecal pellets were characterized by shape as ellipsoid (includes spherical/ovoid— typically appendicularians and typically small crustaceans), cylindrical (typically crustaceans), and tabular (generally considered to be from salps, as in Wilson et al., 2008). Tabular fecal pellets were defined as densely tabular-shaped packed particles with less-defined edges that did not appear to have been encased in a chitinous membrane. Cylindrical, ellipsoid, and ovoid/spheroid fecal pellets all had smooth edges.

A subset of ellipsoid (n = 149) and cylindrical (n = 78) fecal pellets within SES images was manually characterized and measured. Tabular fecal pellets were counted and measured in all SES images (n = 2053). Length and widths of observed pellets were manually measured using FIJI (ImageJ) software (Schindelin et al., 2012). For tabular pellets, lengths and widths were used to calculate pellet volume using the volume formula for a rectangular cuboid shape:

$$\text{Tabular volume} = \left(\frac{1}{4}\,\text{w}\right)\text{lw}$$

where w = width and l = length. Tabular depth values were calculated to be 1/4 the measured width based on the measurements of fresh salp pellets (SEW, pers. obs.). The image pixel area of each manually measured cylindrical pellet was calculated as a rectangle.

$$\text{Cylindrical pellet 2-dimensional area} = \text{l w}$$

The image pixel area of each manually measured ellipsoid pellet was calculated as a 2-dimensional ellipse.

$$\text{Ellipsoid pellet 2} - \text{dimensional area} = \pi \cdot \frac{l}{2} \cdot \frac{w}{2}$$

Pellet image areas were then used to calculate the equivalent spherical diameter (ESD). The linear relationship of measured width versus ESD was determined for cylindrical (0.32 mm mm^{-1}, $R^2 = 0.32$) and ellipsoid (0.7 mm mm^{-1}, $R^2 = 0.83$) pellets (Supplemental Fig. 1). This relationship was used to estimate the pellet width and length of ellipsoid and cylindrical pellets detected and measured in all SES images by the automated image processing method, whose ESDs were determined by measured particle pixel areas. This approach was used to estimate true pellet dimensions because the width and length parameters automatically measured by the image processing functions (e.g. minor and major axes lengths) did not accurately reflect the dimensions of curved or curled pellets. The estimated length and width of each pellet was used to calculate their ellipsoid or cylindrical volume using the following equations,

$$\text{Ellipsoid volume} = \frac{1}{6} \cdot \pi \text{l w}^2$$

$$\text{Cylinder volume} = \pi \left(\frac{w}{2}\right)^2 \text{l}$$

where l = length and w = width. Aggregate volumes were not modeled from SES images because they most likely lost their 3-dimensional shape when they landed on the imaging plate and instead were more similar to a thin film than a spherical aggregate. Measured surface area of SES-imaged aggregates was used in further calculations.

Tabular fecal pellets collected and preserved in the conventional sediment trap samples were counted and retained in bulk samples prior to sample splitting and carbon analysis.

2.2.3. Particle quality: particulate organic carbon (POC) flux and fluorescence

Three measurements served as proxies for particle quality as food: POC flux estimated for particles enumerated using SES macro images (hereafter referred to as POC_{SES} flux), POC flux measured from conventional sediment trap samples (hereafter referred to as POC_{trap} flux), and fluorescence indicators of phytopigments, which are important nutrients to deep-sea megafauna (Wigham et al., 2003) and indicative of material packaged recently in surface waters (Thiel et al., 1989; Agusti et al., 2015).

The following equations were used to model POC_{SES} of aggregates and fecal pellets detected by the SES:

$$\text{Aggregate } POC_{SES}\text{: } C = a * (SA)^b$$

$$\text{Cylindrical and ellipsoid fecal pellet } POC_{SES}\text{: } C = d * V$$

$$\text{Tabular fecal pellet } POC_{SES}\text{: } C = (0.033 \text{ mg mm}^{-3}) * V$$

where C = mg organic carbon, SA = measured aggregate surface area (μm^2), V = estimated fecal pellet volume (mm^3), a = modeled aggregate organic carbon concentration scalar parameter (mg C μm^{-2}), b = modeled slope parameter of aggregate organic carbon to surface area relationship, d = fecal pellet organic carbon concentration scalar parameter (mg C mm^{-3}). Tabular pellet volumes were converted to organic carbon using a conversion factor of 0.033 mg C mm^{-3}, a value close to or the same as those measured across multiple studies (Bruland and Silver, 1981; Manno et al., 2015; Iversen et al., 2017; SEW, unpublished data). Aggregate POC_{SES} was modeled based on a modified version of the power law relationship determined by Alldredge (1998). The cylindrical and ellipsoid fecal pellet scaling parameter (d) was modeled due to the large variation in measured fecal pellet organic carbon contents (Urban-Rich et al., 1998; González and Smetacek, 1994;

Lundsgaard and Olesen, 1997; Reigstad et al., 2005). POC_{SES} flux was modeled per particle type by the following equations:

$$POC_{SES}\_daily\_2h\_mean = \frac{\sum_i^n [\text{aggregate POC}]_i + [\text{ellipsoid pellet POC}]_i + [\text{cylindrical pellet POC}]_i + [\text{tabular pellet POC}]_i}{n}$$

$$POC_{SES}\ flux = \frac{12\ (POCSES\_daily\_2hr\_mean)}{0.5}$$

where i = each image collected every 2 h and n = number of images collected in a 24-h period. Flux was calculated by multiplying the average 2-h POC detected each day by 12 to scale up to 24 h and dividing by the trap collection area (0.5 m^2). Due to the large natural variability often observed in parameter values a, b, and d (Alldredge, 1998; Urban-Rich et al., 1998; González and Smetacek, 1994; Lundsgaard and Olesen, 1997; Reigstad et al., 2005), these parameters were modeled using four approaches. For the first approach, parameters a, b, and d were modeled based on the least-squares best fit values describing log-transformed POC fluxes measured from samples collected by the co-deployed conventional sediment trap containing formalin (see below; "model 1", a = 0.048 *10^{-6} mg μm^{-2}, b = 0.81, d = 0.005 mg mm^{-3}). The best fit value of d was lower than the typical range of values reported in the literature (0.01–0.15 mg C mm^{-3}, Urban-Rich et al., 1998; González and Smetacek, 1994; Lundsgaard and Olesen, 1997; Reigstad et al., 2005). This may reflect a true difference in carbon content of deep-ocean zooplankton pellets, poorly parameterized fecal pellet carbon concentrations, or the limitations of parameterizing aggregates by their 2-dimensional area. To test the sensitivity of the results to the value of the fecal parameter, d was defined as 0.01 mg C mm^{-3} ("model 2"), 0.08 mg C mm^{-3} ("model 3"), or 0.15 mg C mm^{-3} ("model 4") and only the aggregate parameters were modeled by finding the values of a and b resulting in a total SES-estimated POC flux with the least-squares best fit comparison to measured bulk POC flux (model 2: a = 0.043 *10^{-6} mg μm^{-2}, b = 0.81, model 3: a = 0.004 *10^{-6} mg μm^{-2}, b = 0.93, model 4: a = 0.0002 *10^{-6} mg μm^{-2}, b = 1.09).

POC_{trap} flux was measured from the same sediment trap sample splits used to measure mass flux. Following salt-corrected mass flux determination, particulate inorganic carbon content was measured using a coulometer (UIC) and subtracted from total carbon content measured using an elemental analyzer (Perkin-Elmer or Exeter Analytical, University of California Santa Barbara Marine Science Institute Analytical Laboratory) to yield POC_{trap} flux (Baldwin et al., 1998).

Prior to macro imaging, the SES fluorometer (McGill et al., 2016) excited samples with blue LED light at 470 nm, and detected emissions at 590 nm and 690 nm center wavelengths with 10 nm bandwidths (hereafter F_{590} and F_{690}). These readings aimed to quantify the phytopigments phycoerythrin and chlorophyll, respectively (Yentsch and Phinney, 1985), which may indicate the presence of fresh surface-derived material. Low readings of these fluorescence values suggest the material may be refractory.

2.3. Potential environmental drivers of particle flux: illumination and benthic boundary layer currents

2.3.1. Environmental conditions

A time series of solar noon at Station M was generated using the R package "suncalc" (Agafonkin and Thieurmel, 2017), and used to calculate the number of hours since solar noon for each SES sample. A time series of relative lunar illumination at the surface throughout the lunar cycle was generated using the R package "lunar" (Lazaridis, 2014). Because this model does not account for cloudiness, it can be considered a proxy for maximum possible nighttime lunar illumination at the surface for a given date, and is referred to here as lunar $illumination_{max}$. Actual lunar illumination may have been lower based on local weather conditions. This model provides insights into the lunar cycle.

A time series of current speeds and directions was generated from data collected by the Benthic Rover. The Benthic Rover is an autonomous seafloor-transiting vehicle equipped with a current meter (Falmouth 2D-ACM) mounted near the front of its upper frame (approximately 1.8 m above the seafloor; Sherman and Smith, 2009). This single-point acoustic current meter has integrated compass and tilt sensors. To save power, the Benthic Rover current meter collected data for one out of every 15 min at a rate of 1 Hz. This duty cycle resulted in a total of 96 min and 5760 current meter samples per day. This computationally expensive dataset was double decimated. Due to the paucity of significant geological features in the abyssal plain at Station M (Fig. 1), the benthic-boundary-layer currents measured by the Benthic Rover are considered to be representative of broad-scale current patterns at the locations of instruments that collected data for this study.

2.3.2. Data analysis

Generalized Additive Models [GAMs; R package "mgcv" (Wood, 2011)] were used to evaluate the relationships between POC_{SES} flux, the number of hours since solar noon, lunar $illumination_{max}$, and current speed. GAM is a non-parametric smoothing approach for revealing additive non-linear relationships. It is robust when handling highly skewed datasets with a high number of zeros (Beck and Jackman, 1998), and able to tease apart autocorrelation from other patterns (Baayen et al., 2017). The restricted maximum likelihood (REML) option recommended by Wood (2011) was used with the default degrees of freedom or fewer to avoid overfitting. Modeled relationships were visualized using ggplot (Wickham and Wickham, 2007). Data points used to generate the model were not mapped on the visualization of the model (i.e. figures) if less than 10% of deviance was explained by the model.

In addition to considering tidal influences over patterns revealed by GAMs, we examined the potential for transport of material in prevailing benthic boundary layer currents. Current meter data were used to plot northing (v), easting (u), current speed, and particle trajectories for the duration of the deployment using the R packages "oce" (Kelley et al., 2018) and "OceanView" (Soetaert and Soetaert, 2016). Current meter data were smoothed using a Butterworth low-pass filter in the R package "signal" (Ligges et al., 2015). This approach highlights relative differences in northing and easting. Because this step can eliminate extreme values from a visualization, the measured current velocities were provided as well. SES measurements of particle quantity, type, and quality were then aggregated with current speed and source direction to the nearest hour. Bivariate polar plots were used to illustrate how the magnitude of particle flux attributes varied with current source direction and speed (R package "openair"; Carslaw and Ropkins, 2012).

2.4. Correlations between particle quantity, type, and quality and the seafloor carbon budget

Seafloor community respiration rates were measured by the Benthic Rover during 2-d respirometry incubations conducted sequentially every 10 m along a transect (Fig. 1). Aanderaa optodes measured oxygen depletion in acrylic chambers enclosing 730 cm^2 of sea floor surface.

Respiration rates were converted to estimates of carbon consumption using a respiratory quotient of 0.85 (Smith, 1987; Smith et al., 1997; McGill et al., 2007; Sherman and Smith, 2009). This value, sediment community oxygen consumption (SCOC), has the unit mg C m^{-2} d^{-1}. For further details about methods see Smith et al. (2016).

The maximum lagged correlation between changes in carbon supply (total POC_{SES} flux) and subsequent changes in carbon demand (SCOC) was calculated using the "stats" library (R Core Team, 2019). Data were aggregated to daily scales prior to this cross-correlation analysis. A 90-d window was used in this function, which should have been sufficient to capture variability in lags between benthopelagic and benthic process at this site (Smith et al., 2018). Particle-specific POC_{SES} fluxes were shifted forward by this lag, aggregated to SCOC measurement dates, and this supply-demand time-matched dataset was included in a GAM using the approach above. This approach determined the relative correlation of each particle type's contribution to POC_{SES} flux with bulk carbon consumption patterns. The deviance explained by this model was compared to that explained by a linear relationship between POC_{trap} flux versus SCOC similarly shifted according to lags between these variables.

This same time-shifted dataset was used to calculate the carbon budget balance as follows:

$$\text{Carbon budget balance} = \text{POC flux}_{shifted} - \text{SCOC}$$

This step identified periods of carbon budget surplus and deficit. The influence of each particle type (particle-specific POC_{SES} flux) on the carbon budget $balance_{SES}$ time series was then evaluated using GAM. This approach assumes no attenuation of carbon as material sinks from 50 mab (meters above bottom) to the sea floor. The deviance explained by this GAM model was then compared to that explained by the linear relationship between POC_{trap} $flux_{shifted}$ and carbon budget $balance_{trap}$.

3. Results

3.1. Detailed views of particle flux (quantity, type, and quality)

3.1.1. Particle quantity: light attenuation, mass flux, and detrital aggregates on the sea floor

For most periods, light attenuation and mass flux observed from separate sampling platforms showed a similar pattern: low values through March 2015, a steady rise in early March 2015, and elevated values in the spring and summer of 2015 (Fig. 2A, B). These sampling methods diverged considerably for one 10-d period (14–23 April 2015), when mass flux was notably higher than the relative pattern in light attenuation, and another when mass flux was very low.

Phytodetrital aggregates were visible on the sea floor at very low coverage in November 2014 and April–June 2015 (Fig. 2G), with a peak in mid-May that followed the peak in mass flux collected by the conventional sediment trap. Gelatinous detrital aggregate cover did not exceed 1% at any time during the sampling period.

3.1.2. Particle type: fecal pellets and aggregates

The relative contribution of aggregates and fecal pellets to POC_{SES} flux varied over hours to seasons (Fig. 2, Supplemental Figs. 2–5), demonstrating change in the biological mechanisms governing export. Ellipsoid fecal pellets were the most abundant discrete particles detected by the SES from October 2014 through mid-April 2015 (Fig. 2C). A large deposition of tabular fecal pellets began on 30 April 2015 and lasted 30 days, peaking in mid-May 2015. Following this event, total particle number flux dropped to pre-May levels, but with an increased representation of cylindrical fecal pellets compared to ellipsoid fecal pellets. Some of the cylindrical fecal pellets imaged were long and had irregular diameters; given these characteristics they could have been produced by midwater fishes instead of crustaceans (Supplemental Fig. 6; B. Robison, personal communication). Discrete aggregates could not be differentiated consistently due to the collection method, and were not included in this presentation of particle number flux.

Tabular fecal pellets were visible in the conventional sediment trap samples (Fig. 2E), showing peaks of fewer than 3 pellets m^{-2} d^{-1} in February and May 2015. These peaks were earlier and lower-magnitude than peaks in tabular fecal pellet number flux identified from SES images (Fig. 2B).

3.1.3. Particle quality: particulate organic carbon flux and fluorescence

The four POC_{SES} flux modeling approaches compared similarly to measured POC_{trap} flux (Supplemental Fig. 7) according to the root-mean-squared difference (RMSD) between measured and SES-estimated values (model 1 = 9.29 mg C m^{-2} d^{-1}, model 2 = 9.28 mg C m^{-2} d^{-1}, model 3 = 9.30 mg C m^{-2} d^{-1}, model 4 = 9.33 mg C m^{-2} d^{-1}). Three data points differed by more than 15 mg C m^{-2} d^{-1} at the end of the time series, when tabular fecal pellets dominated flux. When these points were excluded, POC flux was best estimated by models 1, 2, and 3 (RMSD of 1.89 mg C m^{-2} d^{-1}, 1.91 mg C m^{-2} d^{-1}, and 2.19 mg C m^{-2} d^{-1}, respectively), and the worst by model 4 (RMSD of 2.63 mg C m^{-2} d^{-1}). The choice of model parameters primarily affected the apparent contribution of cylindrical fecal pellets to total models POC_{SES} fluxes and in turn reduced the relative contribution of aggregates to total modeled POC_{SES} fluxes. Aggregate contribution to total POC_{SES} flux decreased from 48% to 27% in models 1 to 4 while cylindrical fecal pellet contribution to total POC_{SES} flux increased from 1% to 28% in models 1 to 4. Ellipsoid fecal pellets contributed very little to total POC_{SES} flux in all models (0.2% to 5%) and the relative contribution of salp fecal pellet fluxes changed little among models (40–50%). Due to the mid-range parameter values of model 3, this model parameterization was used for subsequent analysis. The model 3 aggregate parameters (a = 0.004 $*10^{-6}$ mg μm^{-2}, b = 0.93) are realistically comparable to those derived empirically by Alldredge (1998); The carbon content of a 1 mm^2 particle (1.52 μg C) estimated by model 1 is ~1.5 greater than the carbon content of a 1 mm^3 by the parameters of Alldredge (1998) (0.99 μg C) and the slope parameter is substantially steeper (0.92 vs. 0.52). These differences could logically reflect the changes that occur when a 2-D, porous aggregate is flattened onto a 2-D glass plate and porosity is reduced.

From Oct 2014 through Apr 2015, POC_{SES} flux was low and dominated by aggregate POC_{SES} flux, punctuated by scattered tabular-fecal-pellet POC_{SES} flux in Jan and Feb 2015 (Fig. 2D). Tabular fecal pellets were the dominant contributor to POC_{SES} flux from late April to late May 2015. This period represented the peak in total POC_{SES} flux. As tabular-fecal-pellet POC_{SES} flux declined in late May, cylindrical fecal pellets became the dominant source of carbon as flux resumed pre-May levels. For most paired sampling periods, POC_{trap} flux was within one standard deviation of average POC_{SES} flux (Fig. 2E). The disparity between POC_{trap} flux and POC_{SES} flux was strongest in late April (when POC_{trap} flux peaked) through early May (when POC_{SES} flux peaked).

Fluorescence indicative of chlorophyll (F_{690}) mirrored the pattern of total POC_{SES} flux with low levels through late April 2015, peaking in mid-May, and returning to pre-May levels in June (Fig. 2F). Fluorescence indicative of phycoerythrin (F_{590}) showed little variability, and was not analyzed further. It rose slightly in May 2015.

3.2. Potential environmental drivers of particle flux: illumination and benthic boundary layer currents

POC_{SES} flux compared to hours since solar noon, lunar $illumination_{max}$, and current speeds (Fig. 3) using GAMs indicated different sources and transport mechanisms for each particle type (Fig. 4, Table 1). The GAM model revealed significantly higher modeled aggregate POC_{SES} flux when currents were slow ($p < 0.05$), and during low and high lunar $illumination_{max}$ ($p < 0.01$). By contrast this model revealed significantly lower modeled aggregate POC_{SES} flux during periods of moderate lunar $illumination_{max}$. The cycles examined here explained 1.47% of deviance in aggregate POC_{SES} flux. Modeled tabular-

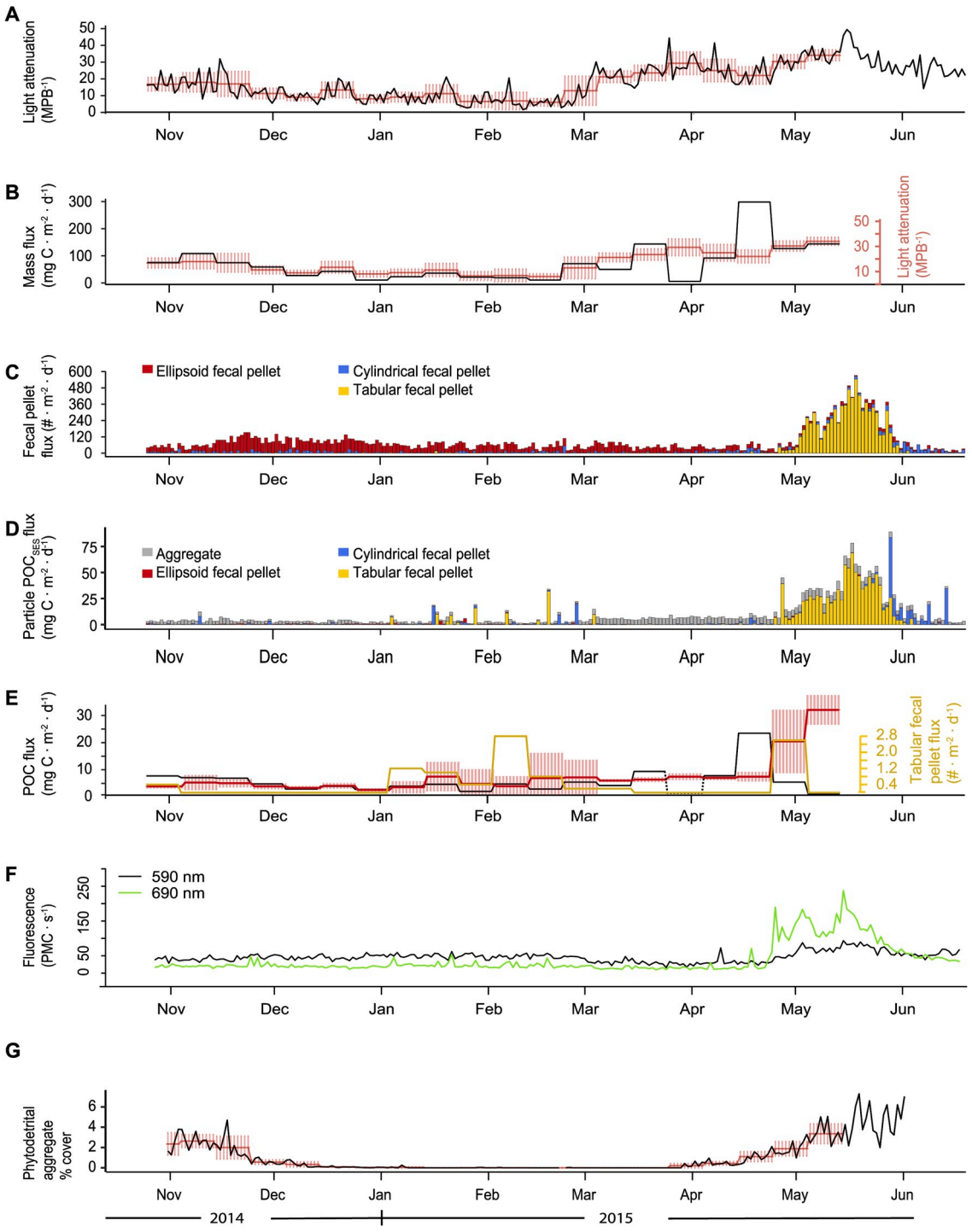

Fig. 2. Particle quantity, type, and quality as measured using the SES, a conventional sediment trap, and time-lapse images of the seafloor. A) SES light attenuation 1 d average (black line) and 10 d average ± s.d. (red line with pink shading) when aggregated to same time scale as conventional sediment trap measurements. B) Mass flux from conventional sediment trap (black line), and light attenuation aggregated to same time scale as conventional sediment trap flux measurements (red line and pink shading = 10 d average ± s.d). C) Contribution of different fecal pellet types to fecal pellet number flux depicted in stacked bar plot (daily average: cylindrical = blue, ellipsoid = red, tabular = yellow). During high flux periods, aggregates often occluded image area and reduced ability to detect absolute fecal pellet number fluxes. D) Stacked bar plot of SES-estimated particulate organic carbon flux (POC_{SES} flux using model 3) by particle type (daily average: aggregate = gray, cylindrical = blue, ellipsoid = red, tabular = yellow). E) POC_{trap} flux (black line = sediment trap measurements) and total POC_{SES} flux aggregated to the same time scale as POC_{trap} flux measurements (red line and pink shading = 10 d average ± s.d.). Tabular fecal pellet number flux from conventional sediment trap (yellow line, right axis). F) SES fluorescence (F_{690}, F_{590}) daily average. G) Daily measurements of percent cover of phytodetrital aggregates on the sea floor. In panel E, dashed line indicates sample too small for analysis.

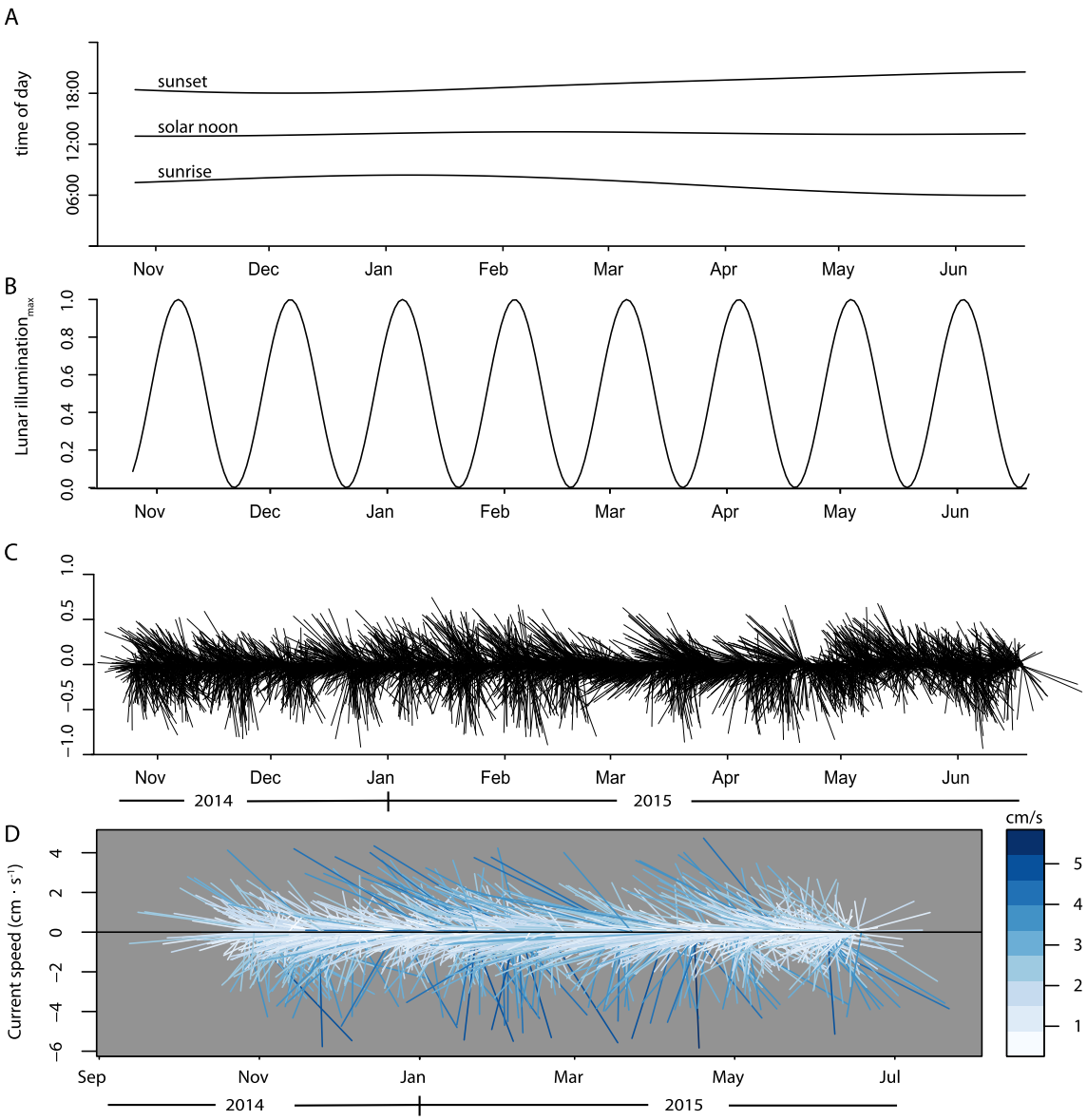

Fig. 3. Potential cyclical environmental drivers of particle transport. A) Sunrise, sunset, and solar noon times. Daylight saving time at local time zone has been removed. B) Modeled surface lunar illumination$_{max}$. C) Stick plot of *v* (northing) and *u* (easting) current components 2 m above sea floor smoothed (Butterworth). D) Current speed and direction measured 2 m above sea floor.

fecal-pellet POC_{SES} flux was significantly ($p < 0.001$) higher when lunar illumination$_{max}$ was low, which would occur during the new moon, and lower when lunar illumination$_{max}$ was high, as would occur during the full moon. The cycles examined here explained 1.55% of deviance in tabular-fecal-pellet POC_{SES} flux. The GAM model of cylindrical-fecal-pellet POC_{SES} flux showed a diel cycle ($p < 0.1$) that peaked during the middle of the night and pre-dawn hours and was lowest a few hours after noon. The cycles examined here explained only 0.8% of deviance in cylindrical-fecal-pellet POC_{SES} flux. No clear pattern could be discerned for the GAM model of ellipsoid-fecal-pellet POC_{SES} flux, with 0.2% of deviance explained by these cycles.

Prevailing benthic boundary layer currents were to the southwest, with disruptions of this pattern toward the end of the survey, including a clockwise rotation (Fig. 5; Supplemental Fig. 8). Spring-neap cycles in current speed and direction were evident in the beginning of the survey period, but were no longer present in May 2015, when southward currents were reduced (Fig. 3C). The prevailing sources of mass (light attenuation), chlorophyll (F_{690}), and total POC_{SES} flux were from the west. Aggregate POC_{SES} appeared to settle during most easterly current conditions. Tabular-fecal-pellet POC_{SES} and F_{690} had the same patterns of source currents; higher values were detected when currents were strong and from the west. Much lower levels of F_{690} corresponded with strong currents from the northeast and the south. Most cylindrical-fecal-pellet POC_{SES} flux also appeared to be delivered under very restricted current conditions—in this case moderate speeds from the southwest. The directional source of ellipsoid-fecal-pellet POC_{SES} flux was less clear, but included a southwesterly source when currents were strong.

3.3. Correlations between particle quantity, type, and quality and the seafloor carbon budget

SCOC was low through mid-May 2015, and elevated in mid-May through mid-June 2015 (Fig. 6A). This measure of carbon consumption lagged changes in total POC_{SES} flux by 12 d (Spearman $\rho = 0.40$, $p < 0.0001$). Particle-specific POC_{SES} fluxes shifted forward 12 d to align with SCOC explained 72.4% of deviance in SCOC (Table 1, Fig. 6B–E). GAM-modeled SCOC increased insignificantly with high values of aggregate POC_{SES} $flux_{shifted}$, and increased significantly with increasing

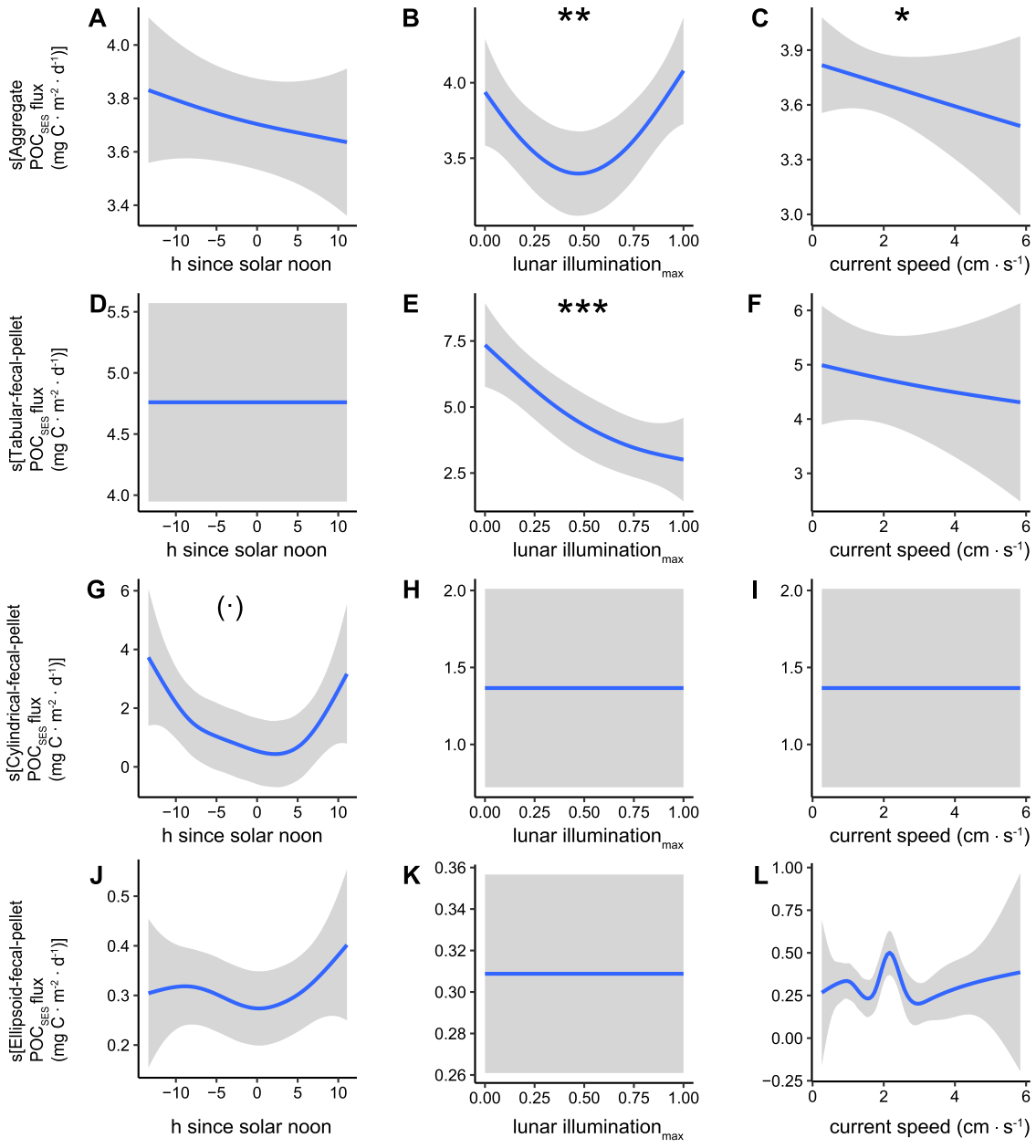

Fig. 4. Relationships between modeled illumination and current speeds and particle-specific POC_{SES} flux depicted by generalized additive models. Modeled relationships (smoothed, s) between (left) hours since solar noon, (middle) modeled surface lunar illumination$_{max}$, and (right) current speed 2 m above the sea floor and A–C) modeled aggregate POC_{SES} flux, D–F) modeled tabular fecal pellet POC_{SES} flux, G–I) modeled cylindrical fecal pellet POC_{SES} flux, and J–L) modeled ellipsoid fecal pellet POC_{SES} flux. Significance codes: 0 '***' 0.001 '**' 0.01 '*' 0.05 '(·)' 0.1 ' ' 1. Solid line = model, shading = 95% confidence band.

cylindrical-fecal-pellet POC_{SES} $flux_{shifted}$ ($p < 0.01$; Fig. 6 B, D). The GAM-modeled relationship between SCOC and tabular-fecal-pellet POC_{SES} $flux_{shifted}$ was significant ($p < 0.001$; Fig. 6C); SCOC increased with moderate tabular-fecal-pellet POC_{SES} $flux_{shifted}$ levels and leveled off with further increases. SCOC decreased insignificantly with increasing ellipsoid-fecal-pellet POC_{SES} $flux_{shifted}$.

A single conventional sediment trap sample (late March through early April 2015) was too small to analyze for POC_{SES} flux. For cross correlation analysis to estimate the lag between changes in POC_{trap} flux and SCOC, this period was given the value of 0.06 mg C m^{-2} d^{-1}, which is the lowest measured value of POC flux for the 50 mab trap recorded at Station M. Based on cross correlation analysis, changes in POC_{trap} flux were followed 32 d later by changes in SCOC ($R^2 = 0.39$).

The seafloor carbon budget ran in deficit for most of the survey period [total carbon budget balance = -12 mg C m^{-2} for aligned carbon supply (POC_{SES} $flux_{shifted}$) and demand (SCOC); Fig. 6F]. A temporary period of carbon surplus was estimated in early May through early June 2015. Particle-specific POC_{SES} $fluxes_{shifted}$ explained 99% of deviance in the carbon budget balance (Table 1), driven by aggregate POC_{SES} $flux_{shifted}$ ($p < 0.001$), tabular-fecal-pellet POC_{SES} $flux_{shifted}$ ($p < 0.001$), and cylindrical-fecal-pellet POC_{SES} $flux_{shifted}$ and ($p < 0.001$; Fig. 6G–J). Relationships between particle-specific POC_{SES} $fluxes_{shifted}$ and the carbon budget balance were superficially similar to those with SCOC except the carbon budget surplus by tabular fecal pellets continued to rise with increasing tabular-fecal-pellet POC_{SES} $flux_{shifted}$ rather than leveling off at moderate values. SCOC and the carbon budget balance changed little with low aggregate POC_{SES} $flux_{shifted}$, but increased steadily with aggregate POC_{SES} flux values above 4–6 mg C m^{-2} d^{-1}.

The linear regression between POC_{trap} flux shifted forward by 32 d, and the carbon budget balance, with values aggregated to the SCOC

Table 1
Results of generalized additive models comparing particle-specific POC_{SES} flux to potential environmental drivers of carbon transport, and aspects of the carbon budget in the benthic boundary layer. Significance codes: 0 '***' 0.001 '**' 0.01 '*' 0.05 '·' 0.1 ' ' 1.

Aggregate POC_{SES} flux ~ s(lunar $illumination_{max}$) + s(hours since solar noon) + s (current speed)		
R^2 = 0.011, Deviance explained = 1.47%, n = 1396		
Smooth terms	F	p-value
lunar $illumination_{max}$	4.2	0.0045 **
hours since solar noon	1.4	0.32
current speed	5.0	0.025 *
Tabular fecal pellet POC_{SES} flux ~ s(lunar $illumination_{max}$) + s(hours since solar noon) + s(current speed)		
R^2 = 0.013, Deviance explained = 1.55%, n = 1396		
Smooth terms	F	p-value
lunar $illumination_{max}$	8.0	0.00016 ***
hours since solar noon	0.24	0.62
current speed	2.6	0.11
Cylindrical fecal pellet POC_{SES} flux ~ s(lunar $illumination_{max}$) + s(hours since solar noon) + s(current speed)		
R^2 = 0.0043, Deviance explained = 0.80%, n = 1396		
Smooth terms	F	p-value
lunar $illumination_{max}$	0.53	0.54
hours since solar noon	2.2	0.09 ·
current speed	0.61	0.61
Ellipsoid fecal pellet POC_{SES} flux ~ s(lunar $illumination_{max}$) + s(hours since solar noon) + s(current speed)		
R^2 = - 0.00062, Deviance explained = 0.20%, n = 1396		
Smooth terms	F	p-value
lunar $illumination_{max}$	0.79	0.37
hours since solar noon	0.57	0.65
current speed	0.051	0.82
SCOC ~ s(shifted aggregate POC_{SES} flux, k = 4) + s(shifted tabular fecal pellet POC_{SES} flux, k = 7) + s(shifted cylindrical fecal pellet POC_{SES} flux, k = 4) + s (shifted ellipsoid fecal pellet POC_{SES} flux, k = 4)		
R2 = 0.68, Deviance explained = 72.4%, n = 58		
Smooth terms	F	p-value
shifted aggregate POC_{SES} flux	0.14	0.84
shifted tabular fecal pellet POC_{SES} flux	9.4	5.8e-07 ***
shifted cylindrical fecal pellet POC_{SES} flux	2.1	0.0067 **
shifted ellipsoid fecal pellet POC_{SES} flux	0.66	0.42
Carbon budget balance ~ s(shifted aggregate POC_{SES} flux) + s(shifted tabular fecal pellet POC_{SES} flux) + s(shifted cylindrical fecal pellet POC_{SES} flux) + s (shifted ellipsoid fecal pellet POC_{SES} flux)		
R^2 = 0.99 , Deviance explained = 98.8%, n = 58		
Smooth terms	F	p-value
shifted aggregate POC_{SES} flux	24	2.6e-08 ***
shifted tabular fecal pellet POC_{SES} flux	220	<2e-16 ***
shifted cylindrical fecal pellet POC_{SES} flux	116	<1.1e-06 ***
shifted ellipsoid fecal pellet POC_{SES} flux	1.4	0.18

sampling schedule explained 67% of variation in this relationship (R^2 = 0.67).

4. Discussion

4.1. Particle flux to the abyssal benthic boundary layer: temporal indicators of transport mechanisms and correlation with the seafloor carbon budget

As predicted, particles packaged in the upper water column (in this case salp fecal pellets) and reaching the benthic boundary layer in fresh condition significantly correlated with SCOC and made the most important modeled contributors to carbon surplus in the abyssal benthic boundary layer. Relationships between illumination cycles, current characteristics, and particle-specific POC_{SES} fluxes revealed useful perspectives into particle sources, even if the temporal cycles analyzed here did not explain a large degree of variance. Salp (tabular) fecal pellets (section *4.1.1.*) appeared to deliver the peaks in fresh surface chlorophyll, and had the strongest modeled correlations with SCOC and the carbon budget balance. Salp-fecal-pellet POC_{SES} flux correlated with lunar $illumination_{max}$. Cylindrical-fecal-pellet POC_{SES} flux (section *4.1.2.*) also correlated significantly with SCOC and the carbon budget balance. A small fraction of these particles may have been produced and actively transported by vertical migrators, indicated by a weak diel cycle of their POC flux. Relationships between aggregate POC_{SES} flux, lunar illumination, and prevailing benthic boundary layer current patterns (section *4.1.3*) suggest most, but not all, aggregates were lower-quality material laterally advected to the site. Ellipsoid fecal pellets (section *4.1.4*) also appear to have represented refractory material. However, elevated SCOC and carbon budget surplus were associated with aggregate POC_{SES} flux exceeding 4 mg C m^{-2} d^{-1}, suggesting some degree of freshness in some aggregates.

Assessing inputs by particle type better quantified the balance of POC flux and SCOC at Station M, and identified approaches to make further methodological refinements. Particle-specific POC_{SES} flux explained over 70% of deviance in SCOC, and over 95% of the deviance in the carbon budget balance. By contrast, POC_{trap} flux explained 39% of variance in SCOC and 67% of variance in the carbon budget balance. Refinements of carbon conversion models may improve these estimates. For example, all cylindrical fecal pellets were treated the same by the methods used here. Their different sources and transport mechanisms may explain the very different parameters used for cylindrical fecal pellet carbon conversions in image analysis studies. Future efforts may focus on differentiating a wider variety of particle types, such as gelatinous material, and incorporating flexible carbon conversion factors that vary with particle attributes such as size (Iversen et al., 2017) and color, and metadata including temporal indicators of transport mechanisms.

4.1.1. Salp fecal pellets: significant correlation with the carbon budget, and possible lunar influence

Since the advent of sediment trap studies, salps have been considered important contributors to carbon export from surface waters and flux to the deep sea (Iseki, 1981; Matsueda et al., 1986; Wilson et al., 2013; Smith et al., 2014). With some of the highest filtration rates known for pelagic zooplankton (Alldredge and Madin, 1982; but see Katija et al., 2017), they consume significant quantities of surface production. Their fast-sinking fecal pellets (Bruland and Silver, 1981) can reach abyssal depths in days, and likely retain most of their original carbon (Caron et al., 1989). Salps are considered so important to global ocean carbon budgets that Henschke et al. (2016) called for them "to be explicitly included in numerical models separate from zooplankton." Our results support those views. Salp fecal pellets delivered an estimated 45% of the total POC_{SES} flux to the benthic boundary layer over an 8-month period based on 2 h resolution data from the SES. They delivered 74% of the carbon flux during temporary carbon surplus periods (Fig. 6). Salp fecal pellets appeared to be the primary source of chlorophyll peaks at the site (Fig. 5), and were the type most strongly correlated with elevated SCOC (Fig. 2). These results suggest salp fecal pellets were the freshest, highest-quality food source available at the time of this study. However, the salp fecal pellet relationship with carbon demand was not linear. Elevated SCOC was associated with moderate increases in salp-fecal-pellet POC_{SES} flux. Additions beyond this point were associated with carbon surplus rather than further consumption (Fig. 6C, H). Future studies are needed to understand the water column conditions that enabled such large quantities of salp fecal pellets to sink intact, which is not guaranteed based on high salp fecal pellet production in surface waters alone (see Iversen et al., 2017).

The ability to resolve and measure individual salp fecal pellets from SES images taken in situ within 2 h of collection, and apply size-based carbon conversions, may explain why estimated contributions of salp fecal pellets to POC flux were much greater in this study compared to

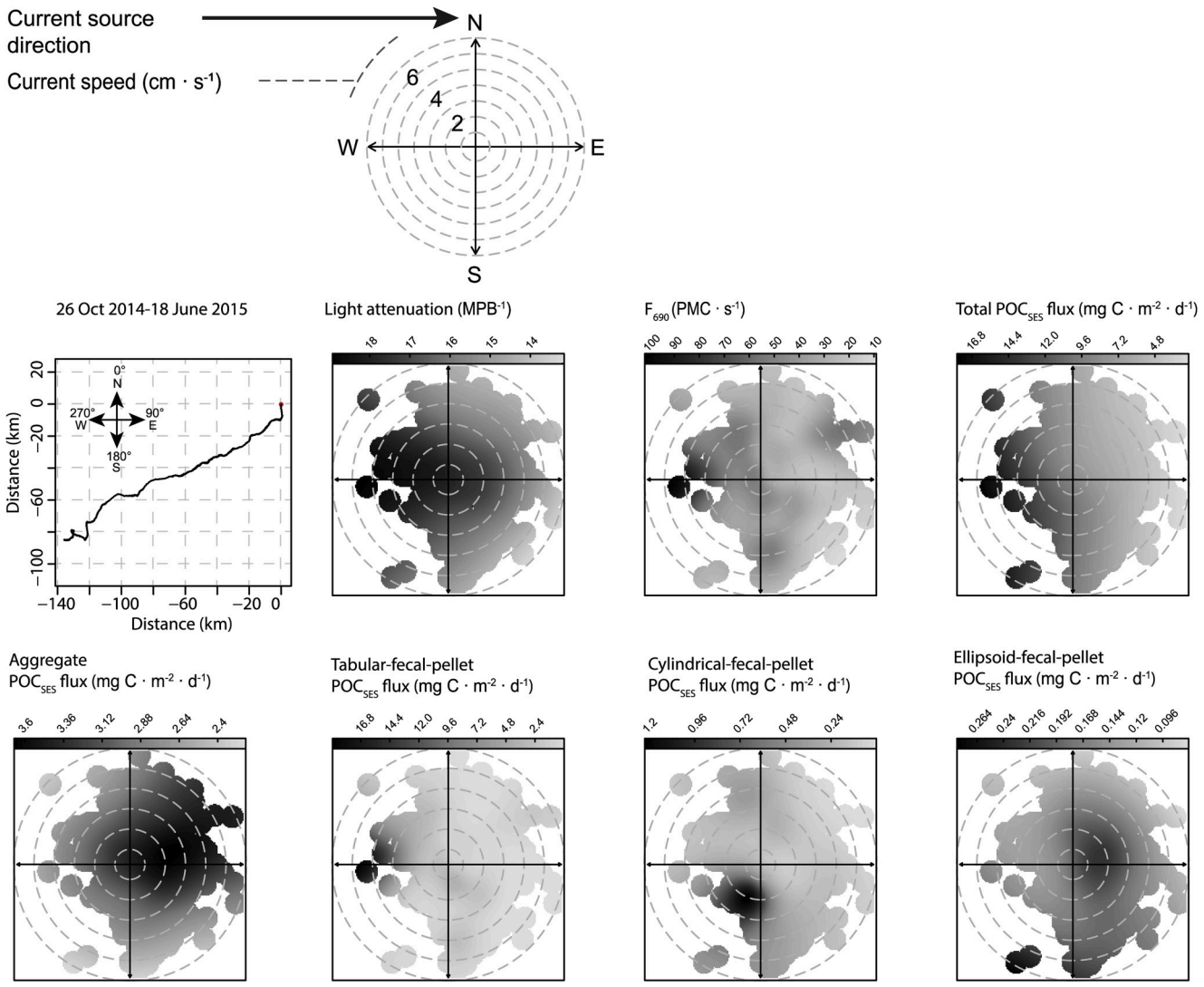

Fig. 5. Indicators of SES-estimated particulate organic carbon (POC_{SES}) physical transport in the benthic boundary layer. Upper left) Particle trajectory plot based on Benthic Rover current meter readings, red dot = point of origin (Supplemental Fig. 8 shows monthly views), Remaining plots) Bivariate polar plots illustrating current source direction and speed associated with POC_{SES} flux parameters (legend at top). All scales were generated automatically by R. (For interpretation of the references to color in this figure legend, the reader is referred to the Web version of this article.)

prior work at Station M (Wilson et al., 2013; Smith et al., 2014). The number of tabular (salp) fecal pellets detected in SES images far exceeded the number individually resolvable in the bulk collection cups of the conventional sediment trap, and these two methods detected different timing in peak salp fecal pellet number flux. These differences may be due to the relatively disruptive nature of bulk sampling methods and the extended storage time in sampling cups of conventional sediment traps prior to recovery (between ~1 and ~34 weeks in this study). Wilson et al. (2013) also reported difficulty resolving salp fecal pellets in preserved bulk sediment trap samples, which precluded direct measurement of their contribution to total POC flux. Instead, prior studies at Station M (Wilson et al., 2013; Smith et al., 2014) have used a single carbon conversion factor (119 mg C pellet $^{-1}$; Madin, 1982) for all salp fecal pellets counted, regardless of fecal pellet size. Other possible reasons for the differences in tabular-fecal-pellet number fluxes recorded by these two traps are explored in section 4.3.

Estimating and predicting the role of salps in the global ocean carbon budget will require understanding the environmental controls of their populations. A strong lunar cycle was found in salp-fecal-pellet POC flux to 3900 m. Most of this flux occurred during a single month spanning a new moon. It is possible that these results stemmed from a month-long salp bloom driven by increased availability of surface plankton (Silver, 1975), which we did not study, and that the timing was not related. Our results may instead be from the slow passage of a large, persistent surface bloom of salps over Station M. Large salp blooms lasting several months do occur in the CCE (Berner, 1967). The consistent current source of most salp-fecal-pellet POC_{SES} flux (Fig. 5) may raise the question whether this scenario is likely in this case. Regardless of bloom size and evolution, salp fecal pellets sampled by the SES likely sank from a very restricted surface region, as predicted for modeled fast-sinking particles detected at depth at Station M (Ruhl et al., 2020). Lunar control of spawning activity may provide an alternate explanation. Time-series studies of salp populations often present monthly-resolution data (e.g. Liu et al., 2012; Stone and Steinberg, 2014), which prevents assessment of lunar control over salp abundance or feeding activity. Inconsistent reactions of salps to light (Sasikumar et al., 2014; Purcell and Madin, 1991) and vertical migrations (including reverse migrations) suggest their movements in relation to surface illumination involve more than just predator avoidance and feeding migrations (Stone and Steinberg, 2014; Purcell and Madin, 1991; Pascual et al., 2017). Pascual et al. (2017) documented a spawning aggregation of *Salpa fusiformis* around the new moon. As found here, peaks in salp-fecal-pellet flux at

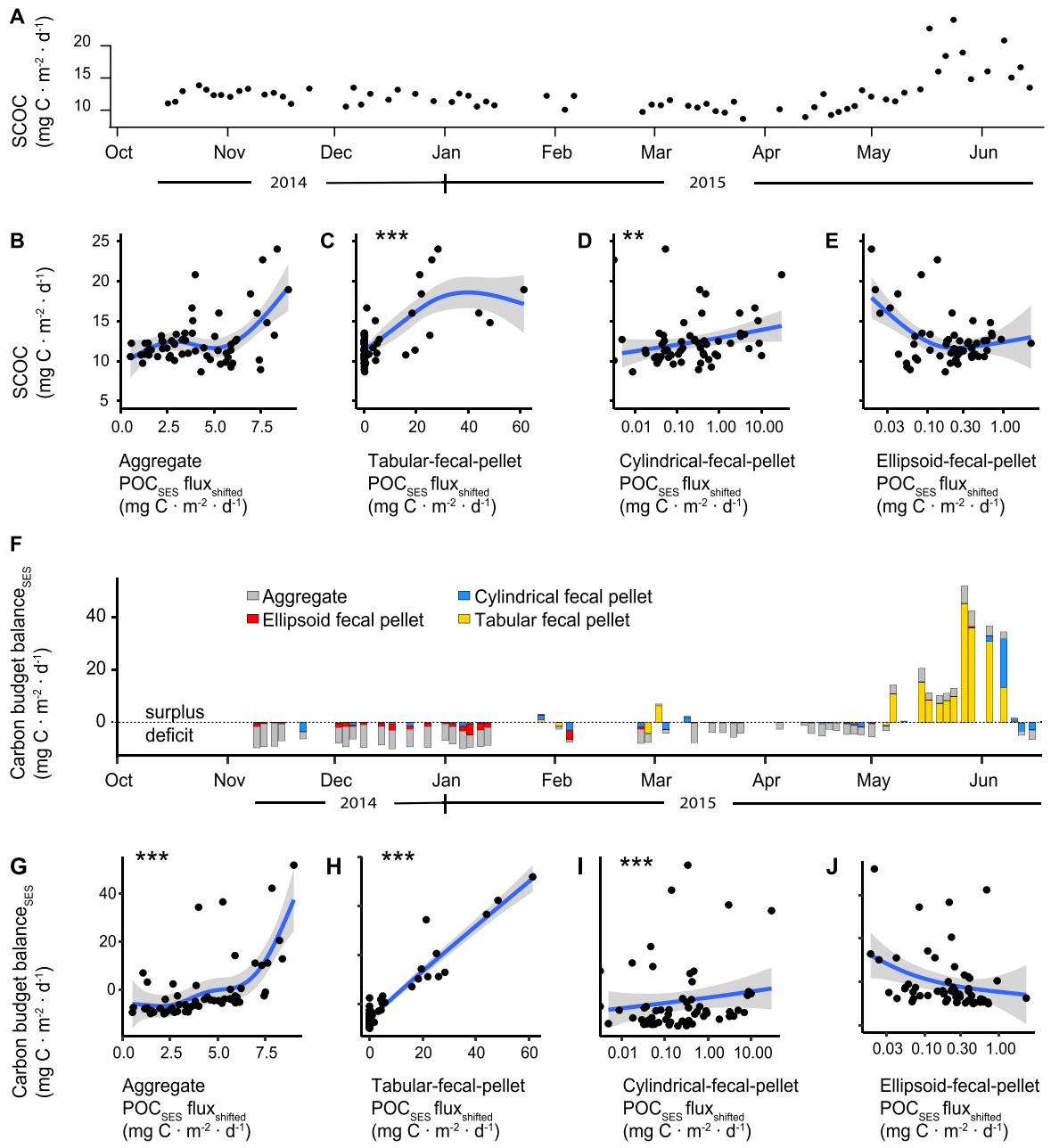

Fig. 6. Relationships between particle quantity, type, and quality and the seafloor carbon budget. A) Carbon demand [Sediment community oxygen consumption (SCOC)]. B–D) Generalized additive models showing influence of POC_{SES} flux via B) aggregates, C) tabular fecal pellets, D) cylindrical fecal pellets, and E) ellipsoid fecal pellets on SCOC, F) Seafloor carbon budget balance [Carbon supply (total POC_{SES} flux) minus carbon demand (SCOC); supply and demand time series were temporally aligned (forward shift of carbon supply by 12 d, determined as the lag with peak correlation in cross-correlation analysis)] by particle type (aggregate = gray, cylindrical = blue, ellipsoid = red, tabular = yellow). G–J) Generalized additive models showing influence of POC_{SES} flux via G) aggregates, H) tabular fecal pellets, I) cylindrical fecal pellets, and J) ellipsoid fecal pellets on the carbon budget balance. Significance codes: *** = $p < 0.001$, ** = $p < 0.01$. Solid line = model, shading = 95% confidence band. D, E, I, J use a log scale for the x-axis.

Station M in 2012 overlapped with, or were close to, the new moon (Smith et al., 2014). Predicting any impact of salp aggregations on carbon export and sequestration will require species-specific studies to understand the timing of aggregation, spawning, and influences of reproduction on feeding. For example, *Cyclosalpa bakeri* spawning aggregations are governed by lunar illumination, but centered around the full moon, and individuals appear to cease feeding temporarily while spawning (Purcell and Madin, 1991).

4.1.2. *Cylindrical fecal pellets: significant correlation with the carbon budget, and with a diel cycle*

Cylindrical fecal pellets were important contributors of carbon flux at Station M. They contributed 17% of total POC_{SES} flux, and 10% of carbon flux during periods of carbon surplus. Previous work found that cylindrical-fecal-pellet flux correlated significantly with POC flux over a 15-y time series at Station M (Wilson et al., 2013). Like Wilson et al. (2013), we found the highest cylindrical-fecal-pellet fluxes in the summer.

Given the contribution of cylindrical fecal pellets to the carbon budget balance, it is important to know their source. In general, most

cylindrical fecal pellets collected at abyssal depths are assumed to be produced by crustaceans feeding in the bathypelagic zone (Wilson et al., 2013). This may be true for most of the cylindrical fecal pellets recorded here. However, the morphology of some cylindrical fecal pellets suggests a small fraction may have other sources. Very long, fragile, and irregularly-shaped fecal pellets may have been produced instead by fishes (Robison, personal communication). We do not know which organisms imparted a weak diel cycle in cylindrical-fecal-pellet POC_{SES} flux. Some midwater fishes in the CCE, including the myctophid *Stenobrachius leucopsarus*, can vertically migrate (Watanabe et al., 1999) and produce fecal pellets that sink at rates of 1 km d^{-1} (Robison and Bailey, 1981). Zooplankton and fishes living in the bathypelagic and deeper are not generally considered diel vertical migrators (Burd et al., 2010; Childress et al., 1980). Still, the bathypelagic fish *Cyclothone acclinidens* exhibits a diel cycle in respiration even if its population does not vertically migrate (Smith and Laver, 1981); feeding and fecal pellet production in this species could exhibit a similar pattern. It is also possible that the observed fecal pellets were produced by deep-water organisms that interact trophically with shallower diel vertical migrators, possibly making small upward migrations, rather than being exposed to illumination cycles themselves. Depth-tiered diel vertical migrations, in which zooplankton take part in a "bucket brigade" of carbon transfer through feeding and defecation, can extend at least to 1200 m, beyond the reaches of surface illumination (Ochoa et al., 2013). These interactions are similar to Vinogradov's "*migration ladder*" (1970) and Bollens et al.'s (2010) "*cascading migrations*" but do not necessarily involve predator-prey interactions. Additional data are required to evaluate these hypotheses and understand their possible influences on carbon transport. Extended observations over multiple years and more detailed classification of cylindrical pellet types are necessary to determine whether the trace signal of diel periodicity observed here reflects a true ecological mechanism of flux at abyssal depths.

4.1.3. Aggregates: minor contributor to carbon surplus, and evidence for transport in currents

Most, but not all, aggregates appeared to be low-quality particles sourced from lateral-advection, and possibly local rebound of recently-settled detritus, rather than fresh surface export. If some of these aggregates had been packaged in surface waters, then they appear to have been exposed to impactful carbon attenuation processes as they sank, possibly slowly, through the water column. Aggregates were consistent components of particle flux to the benthic boundary layer, and they contributed 36% of total POC_{SES} flux, and 15% of POC_{SES} flux during the carbon surplus period. Time series plots (Fig. 2) and bivariate polar plots (Fig. 5) showed little correspondence between aggregate POC_{SES} flux and elevated F_{690} (chlorophyll). Aggregates settled during all current flow conditions, but the primary source was the prevailing northeasterly current, which overlapped to a minor degree with sources of low F_{690}. This result supports previous evidence that resuspended material laterally advects to Station M from the continental margin (Hwang et al., 2004, 2005). However, not all aggregate material may be sourced from upslope. Correlations with lunar $illumination_{max}$ and current speeds (Fig. 4B) indicate local rebound and resettling of material with tidal oscillations (especially spring/neap), as identified in the benthic boundary layer at the Porcupine Abyssal Plain (Turnewitsch et al., 2017). While currents used in the decimated dataset in our analyses did not exceed thresholds considered necessary for local rebound of freshly settled aggregates (7.8 cm s^{-1}; Beaulieu and Baldwin, 1998), this threshold was exceeded at one point in the raw current meter dataset. Additionally, local resuspension can occur at much slower current speeds during semi-diurnal tidal oscillations (e.g. Turnewitsch et al., 2017; Vangriesheim et al., 2001). It is possible that some of these aggregates were packaged higher in the water column, and degraded as they sank slowly to the benthic boundary layer. Finally, some aggregates associated with POC_{SES} flux above 4–6 mg C m^{-2} d^{-1} may have carried fresher material, and contributed to elevations in SCOC and the carbon budget balance. Future investigations may examine sources of variation in aggregate freshness, and possible seasonal patterns.

Most aggregates documented by the SES in this study differed from the large, fluorescent phytodetrital aggregates that have settled at Station M during periods of very high POC flux (Smith et al., 2014). During those periods, detrital aggregates have covered more than 46% of the sea floor, and were significantly correlated with rapid SCOC responses (Smith et al., 2018). Instead, most aggregates recorded here may be more representative of those settling during less-extreme flux conditions (POC flux $<$ time-series mean $+$ 2 standard deviations; Smith et al., 2018). Phytodetrital aggregates here covered less than 7.3% of the sea floor (Station M time-series mean $=$ 6.4%). Most aggregate POC_{SES} flux was associated with little change in SCOC and the carbon budget balance. Future efforts may focus on further understanding the delivery of small quantities of fresh aggregates like those observed here associated with moderate POC flux values, and correlated with elevated SCOC and carbon budget surpluses.

4.1.4. Ellipsoid fecal pellets: repackaged deep-sea material

Like aggregates, ellipsoid fecal pellets made consistent contributions to the carbon flux for most of the year, but made a minimal contribution to periods of carbon surplus. These results corroborate Wilson et al. (2013) who used long time-series data to reveal that ellipsoid pellets made the highest contribution to organic carbon flux in late fall at Sta. M. No clear association was found between ellipsoid-fecal-pellet POC_{SES} flux and the cyclical environmental drivers assessed here. These results would be consistent with previous views that ellipsoid fecal pellets are repackaged by non-migrating zooplankton, likely appendicularians (Wilson et al., 2008), in the bathypelagic water column. As such, these pellets may have provided an important mechanism for transporting suspended POC to the abyssal seafloor community and increasing the transfer efficiency of sinking POC.

4.2. Advantages of high-temporal-resolution autonomous instrumentation

Most carbon export studies have been conducted using conventional sequencing sediment traps that integrate collections over long periods and are limited by a finite number of sample bottles (McDonnell et al., 2015). This approach misses much-needed temporal information about particle composition and transformation processes (Boyd et al., 2019). A suite of persistent, autonomous seafloor instrumentation including the SES and Benthic Rover (Smith et al., 2017) provided detailed views of carbon flux to abyssal depths that could not be obtained using conventional sediment traps alone. As shown here, autonomous optical technologies like the SES can detect rapid changes in sinking particles to resolve the appropriate time-scales of carbon export and shed light on some of its ecological drivers (Boyd and Newton, 1995; Buesseler et al., 2007).

Moreover, the SES imaging approach enabled sensitive detection and quantification of relatively fragile particles that are often disrupted by conventional collection approaches. Contributions by salp fecal pellets were better resolved when using SES images compared to conventional sediment trap collections. Imaging techniques like those used here may provide tools for quantifying the influence of other delicate particle types on carbon flux to the abyss. For example, because fish fecal pellets are delicate (Robison and Bailey, 1981), difficult to detect, and hard to study from sediment trap collections, their role in carbon export studies may be underappreciated (Saba and Steinberg, 2012). Yet they can play a significant role in the export of surface carbon and nitrogen in upwelling regions including the CCE (Saba and Steinberg, 2012).

Site-specific calibration of optical sediment trap measurements with carbon flux data is necessary to support their widespread use (Alldredge, 1998; McGill et al., 2016; Estapa et al., 2017; Bourne et al., 2019). In most cases the SES accurately represented the quantity of particulate material sinking to 50 mab at Station M. Light attenuation could be used to derive mass flux, as has been found by other studies (Bishop et al.,

2016). Based on upper-ocean calibrations, optical sediment trap light attenuation appears to be well-correlated with conventional sediment trap POC flux measurements (Estapa et al., 2017; Bourne et al., 2019). Bourne et al. (2019) also showed a strong relationship between fecal pellet counts from optical sediment trap images compared to physical samples collected concurrently in the traps. POC_{SES} flux matched POC_{trap} flux values in most cases, but did not perform well in the highest-flux conditions. Possible sources of these differences are explored below.

4.3. Sources of bias

This study modeled particle carbon contents using approaches similar to or slightly modified from those approaches employed in other studies (e.g. Alldredge, 1998; Silver and Gowing, 1991; Wilson et al., 2013). To apply these approaches to the entire particle pool, it was necessary to assume uniform content in each particle category despite variability in composition and origin within individual categories. For example, diatom aggregates can have higher carbon and nitrogen content than larvacean and fecal detritus (Alldredge, 1998), and fecal-pellet carbon content can vary with zooplankton diet (Wilson et al., 2008). Size-based trends in C:N led Alldredge (1998) to conclude that larger aggregates were more refractory than smaller ones. The converse is likely true for salp fecal pellets because large salp fecal pellets sink much faster than small ones (Bruland and Silver, 1981), reducing the time over which degradation can occur. Despite known variability and heterogeneity of particle carbon content, the relatively simplistic modeling approach used here reflected measured POC fluxes within one standard deviation in most cases, and enabled further resolution of those fluxes into particle source. The amount of carbon attributed to each particle type was sensitive to the parameters chosen in the model, and primarily affected the relative contribution of cylindrical fecal pellets, which was compensated for by changes in the modeled contribution of aggregates to POC_{SES} flux. The choice of parameters primarily affects interpretation of results during periods of high cylindrical fecal pellet fluxes, such as the period of June during these observations. These parameterizations could be better constrained by additional years of observation that include more time periods when cylindrical pellets dominate particle fluxes.

Differences between the magnitude and timing of material detected by the SES and conventional sediment trap may reflect a combination of instrument bias and spatial variation. Because not all material could be identified by the SES, it is not surprising that some POC_{SES} flux estimates were lower than concurrent POC_{trap} flux measurements. The image analysis method used here was not designed to detect and identify gelatinous material like pyrosomes and salp carcasses, and this would have led further to underestimates of carbon flux. Although these particle types were not included in the analyses, they were visible in SES images following the peak in tabular-fecal-pellet flux. Additionally, limits on the detection and identification of fecal pellets during high-flux conditions might have influenced results. Fecal pellets were better-resolved in winter when aggregate flux was low and did not mask other material on the slide. Fecal pellet identifications from conventional sediment trap samples are more successful during low-flux periods as well (Wilson et al., 2013). It is also possible that some of the discrepancy between the two collection methods could be due to methodological limitations, including clogging issues in the conventional sediment trap, which have not occurred in the concurrently-deployed SES (McGill et al., 2016). Finally, spatial variation may explain the temporal offsets of flux peaks recorded by the SES and conventional trap. Kilometer-scale variation in detrital aggregate coverage has been documented at Station M (Lauerman et al., 1996). Despite these differences, POC flux estimated using SES images explained variation of SCOC at the seafloor better than the bulk measurements collected by the conventional sediment trap.

This study aimed to understand some of the many mechanisms influencing carbon processing in the benthic boundary layer—not to provide a new generalization of the carbon budget at Station M. It took place during a multi-year marine heatwave (fall 2013–winter 2015) in the Northeast Pacific, with anomalously warm surface waters, low surface pressures (Di Lorenzo and Mantua, 2016), low primary productivity (Gomez-Ocampo et al., 2018), altered epipelagic communities (Sakuma et al., 2016), and relatively low carbon fluxes without a "pulse" event (Smith et al., 2018). Carbon dynamics at Station M show considerable interannual variability (Smith et al., 2013), as do bottom currents (Connolly et al., 2020), which may have been anomalous during this survey (Smith et al., 2020).

5. Conclusions and future directions

Discriminating POC flux by particle type at high temporal resolution provided a detailed view of carbon processing in the abyssal benthic boundary layer. This approach identified salp fecal pellets as the dominant particle type responsible for the seafloor carbon budget surplus in early summer 2015. In situ imaging allowed the study of fragile particles which may be compromised in conventional sediment trap collections and otherwise underappreciated in deep-sea carbon processing studies. By evaluating particle flux in relation to cycling environmental conditions, particle transport mechanisms studied here (e.g. lateral advection and possible active transport) could be discerned. Future efforts may focus on deploying co-located SES and conventional sediment traps for calibration of carbon to volume ratios of different particle types, and across seasonal transitions. Doing so will allow better differentiation of particles in optical sediment trap images, and incorporation of flexible carbon conversion factors that vary with particle attributes, image metadata, and transport mechanisms indicated by temporal cycles of flux. The deployment of multiple optical sediment traps throughout the water column would help disentangle the vertical extent and overlap of physical and biological transport mechanisms above the benthic boundary layer. Longer-term high-temporal-resolution studies using the SES may help link mechanisms acting at hourly to seasonal scales with longer-term forcing by changes in climate (e.g. Smith et al., 2009).

Declaration of competing interest

The authors declare that they have no known competing financial interests or personal relationships that could have appeared to influence the work reported in this paper.

CRediT authorship contribution statement

Christine L. Huffard: Methodology, Data curation, Visualization, Writing - original draft, Writing - review & editing. **Colleen A. Durkin:** Methodology, Data curation, Visualization, Writing - original draft, Writing - review & editing. **Stephanie E. Wilson:** Methodology, Data curation, Writing - original draft, Writing - review & editing. **Paul R. McGill:** Methodology, Data curation, Writing - review & editing. **Rich Henthorn:** Methodology, Data curation, Writing - review & editing. **Kenneth L. Smith:** Methodology, Writing - review & editing, Supervision.

Acknowledgements

Rob Glatts and Fred Uhlman contributed greatly to the early development of the SES at the Scripps Institution of Oceanography funded by NSF (OCE-0002385) to KLS. This current research was supported by the David and Lucile Packard Foundation. CAD was supported by California Sea Grant award R/HCME-37. We thank Alana Sherman, John Ferreira, and Larry Bird for developing the current SES and maintaining the SES, time-lapse camera, and Benthic Rover. The crew of the Research Vessel *Western Flyer* is gratefully acknowledged for supporting field operations. Fig. 1 was prepared by Linda Kuhnz and Mariah Salisbury. This

manuscript was improved by comments from Henry Ruhl and two very helpful anonymous reviewers.

Appendix A. Supplementary data

Supplementary data to this article can be found online at https://doi.org/10.1016/j.dsr2.2020.104763.

References

Agafonkin, V., Thieurmel, B., 2017. Suncalc: Compute Sun Position, Sunlight Phases, Moon Position, and Lunar Phase. R package version 0.3.

Agusti, S., González-Gordillo, J.I., Vaqué, D., Estrada, M., Cerezo, M.I., 2015. Ubiquitous healthy diatoms in the deep sea confirm deep carbon injection by the biological pump. In: Climate Change and the Oceanic Carbon Cycle. Apple Academic Press, pp. 149–172.

Alldredge, A., 1998. The carbon, nitrogen and mass content of marine snow as a function of aggregate size. Deep-Sea Res. Part. I. 45, 529–541.

Alldredge, A.L., Madin, L.P., 1982. Pelagic tunicates: unique herbivores in the marine plankton. Bioscience 32, 655–663.

Baayen, H., Vasishth, S., Kliegl, R., Bates, D., 2017. The cave of shadows: addressing the human factor with generalized additive mixed models. J. Mem. Lang. 94, 206–234.

Baldwin, R.J., Glatts, R.C., Smith Jr., K.L., 1998. Particulate matter fluxes into the benthic boundary layer at a long time-series station in the abyssal NE Pacific: composition and fluxes. Deep-Sea Res. Part II 45, 643–665.

Beaulieu, S., Baldwin, R., 1998. Temporal variability in currents and the benthic boundary layer at an abyssal station off central California. Deep-Sea Res. Part II 45, 587–615.

Beck, N., Jackman, S., 1998. Beyond linearity by default: generalized additive models. Am. J. Polym. Sci. 42, 596.

Belcher, A., Henson, S.A., Manno, C., Hill, S.L., Atkinson, A., Thorpe, S.E., Fretwell, P., Ireland, L., Tarling, G.A., 2019. Krill faecal pellets drive hidden pulses of particulate organic carbon in the marginal ice zone. Nat. Commun. 10, 1–8.

Belcher, A., Manno, C., Ward, P., Henson, S., Sanders, R., Tarling, G., 2017. Copepod faecal pellet transfer through the meso-and bathypelagic layers in the Southern Ocean in spring. Biogeosciences 14, 1511–1525.

Berner, L.D., 1967. Distributional Atlas of Thaliacea in the California Current Region. State of California, Marine Research Committee.

Bishop, J.K., Fong, M.B., Wood, T.J., 2016. Robotic observations of high wintertime carbon export in California coastal waters. Biogeosciences 13, 3109.

Bollens, S.M., Rollwagen-Bollens, G., Quenette, J.A., Bochdansky, A.B., 2010. Cascading migrations and implications for vertical fluxes in pelagic ecosystems. J. Plankton Res. 33, 349–355.

Bourne, H.L., Bishop, J.K.B., Wood, T.J., Loew, T.J., Liu, Y., 2019. Carbon Flux Explorer optical assessment of C, N and P fluxes. Biogeosciences 16, 1249–1264.

Boyd, P.W., Claustre, H., Levy, M., Siegel, D.A., Weber, T., 2019. Multi-faceted particle pumps drive carbon sequestration in the ocean. Nature 568, 327–335.

Boyd, P., Newton, P., 1995. Evidence of the potential influence of planktonic community structure on the interannual variability of particulate organic carbon flux. Deep-Sea Res. Part I 42, 619–639.

Bruland, K.W., Silver, M.W., 1981. Sinking rates of fecal pellets from gelatinous zooplankton (salps, pteropods, doliolids). Mar. Biol. 63, 295–300.

Buesseler, K.O., Lamborg, C.H., Boyd, P.W., Lam, P.J., Trull, T.W., Bidigare, R.R., Bishop, J.K.B., Casciotti, K.L., Dehairs, F., Elskens, M., et al., 2007. Revisiting carbon flux through the ocean's twilight zone. Science 316, 567–570.

Burd, A.B., Hansell, D.A., Steinberg, D.K., Anderson, T.R., Ar\'\istegui, J., Baltar, F., Beaupre, S.R., Buesseler, K.O., DeHairs, F., Jackson, G.A., others, 2010. Assessing the apparent imbalance between geochemical and biochemical indicators of meso-and bathypelagic biological activity: what the@ $♯! is wrong with present calculations of carbon budgets? Deep-Sea Res. Part II 57, 1557–1571.

Caron, D.A., Madin, L.P., Cole, J.J., 1989. Composition and degradation of salp fecal pellets: implications for vertical flux in oceanic environments. J. Mar. Res. 47, 829–850.

Carslaw, D.C., Ropkins, K., 2012. Openair—an R package for air quality data analysis. Environ. Model. Software 27, 52–61.

Cavan, E.L., Le Moigne, F.A.C., Poulton, A.J., Tarling, G.A., Ward, P., Daniels, C.J., Fragoso, G.M., Sanders, R.J., 2015. Attenuation of particulate organic carbon flux in the Scotia Sea, Southern Ocean, is controlled by zooplankton fecal pellets. Geophys. Res. Lett. 42, 821–830.

Childress, J.J., Taylor, S.M., Cailliet, G.M., Price, M.H., 1980. Patterns of growth, energy utilization and reproduction in some meso-and bathypelagic fishes off southern California. Mar. Biol. 61, 27–40.

Christina, L., Passow, U., 2007. Factors influencing the sinking of POC and the efficiency of the biological carbon pump. Deep-Sea Res. Part II 54, 639–658.

Cisewski, B., Strass, V.H., Rhein, M., Krägefsky, S., 2010. Seasonal variation of diel vertical migration of zooplankton from ADCP backscatter time series data in the Lazarev Sea, Antarctica. Deep-Sea Res. Part I 57, 78–94.

Connolly, T.P., McGill, P.R., Henthorn, R.G., Burrier, D.A., Michaud, C., 2020. Near-bottom currents at station M in the abyssal Northeast Pacific. Deep-Sea Res. Part II this volume.

Conte, M.H., Ralph, N., Ross, E.H., 2001. Seasonal and interannual variability in deep ocean particle fluxes at the Oceanic Flux Program (OFP)/Bermuda Atlantic Time Series (BATS) site in the western Sargasso Sea near Bermuda. Deep-Sea Res. Part II 48, 1471–1505.

Danovaro, R., Dell'Anno, A., Fabiano, M., 2001. Bioavailability of organic matter in the sediments of the Porcupine Abyssal Plain, northeastern Atlantic. Mar. Ecol. Prog. Ser. 220, 25–32.

Di Lorenzo, E., Mantua, N., 2016. Multi-year persistence of the 2014/15 North Pacific marine heatwave. Nat. Clim. Change 6, 1042.

Dickens, A.F., Gélinas, Y., Masiello, C.A., Wakeham, S., Hedges, J.I., 2004. Reburial of fossil organic carbon in marine sediments. Nature 427, 336.

Estapa, M., Durkin, C., Buesseler, K., Johnson, R., Feen, M., 2017. Carbon flux from bio-optical profiling floats: calibrating transmissometers for use as optical sediment traps. Deep-Sea Res. Part I 120, 100–111.

Gleiber, M.R., Steinberg, D.K., Ducklow, H.W., 2012. Time series of vertical flux of zooplankton fecal pellets on the continental shelf of the western Antarctic Peninsula. Mar. Ecol. Prog. Ser. 471, 23–36.

Gomez-Ocampo, E., Gaxiola-Castro, G., Durazo, R., Beier, E., 2018. Effects of the 2013-2016 warm anomalies on the California Current phytoplankton. Deep-Sea Res. Part II 151, 64–76.

González, H.E., González, S.R., Brummer, G.A., 1994. Short-term sedimentation pattern on zooplankton, faeces, and microzooplankton at a permanent station in the Bjornafjorden (Norway) during April–May 1992. Mar. Ecol. Prog. Ser. 105, 31–45.

Guidi, L., Stemmann, L., Jackson, G.A., Ibanez, F., Claustre, H., Legendre, L., Picheral, M., Gorskya, G., 2009. Effects of phytoplankton community on production, size, and export of large aggregates: a world-ocean analysis. Limnol. Oceanogr. 54, 1951–1963.

Harding Jr., L.W., Fisher Jr., T.R., Tyler, M.A., 1987. Adaptive responses of photosynthesis in phytoplankton: specificity to time-scale of change in light. Biol. Oceanogr. 4, 403–437.

Henschke, N., Everett, J.D., Richardson, A.J., Suthers, I.M., 2016. Rethinking the role of salps in the ocean. Trends Ecol. Evol. 31, 720–733.

Hwang, J., Druffel, E.R.M., Griffin, S., Smith Jr., K.L., Baldwin, R.J., Bauer, J.E., 2004. Temporal variability of Δ14C and δ13C, and C/N in sinking particulate organic matter at a deep time series station in the northeast Pacific Ocean. Global Biogeochem. Cycles 18.

Hwang, J., Druffel, E.R.M., Komada, T., 2005. Transport of organic carbon from the California coast to the slope region: a study of $\Delta^{14}C$ and $\delta^{13}C$ signatures of organic compound classes. Global Biogeochem. Cycles. Cycles 19.

Iseki, K., 1981. Particulate organic matter transport to the deep sea by salp fecal pellets. Mar. Ecol. Prog. Ser. 5, 55–60.

Isla, A., Scharek, R., Latasa, M., 2015. Zooplankton diel vertical migration and contribution to deep active carbon flux in the NW Mediterranean. J. Mar. Syst. 143, 86–97. https://doi.org/10.1016/j.jmarsys.2014.10.017.

Iversen, M.H., Pakhomov, E.A., Hunt, B.P., v Jagt, H., Wolf-Gladrow, D., Klaas, C., 2017. Sinkers or floaters? Contribution from salp pellets to the export flux during a large bloom event in the Southern Ocean. Deep-Sea Res. Part II 138, 116–125. https://doi.org/10.1016/j.drs2.2016.12.004.

Kahru, M., Goericke, R., Kelly, T.B., Stukel, M.R., 2019. Satellite estimation of carbon export by sinking particles in the California Current calibrated with sediment trap data. Deep-Sea Res. Part. II 104639. This volume.

Kahru, M., Mitchell, B.G., 2002. Influence of the el Niño-La Niña cycle on satellite-derived primary production in the California current. Geophys. Res. Lett. 29, 21–27.

Katija, K., Sherlock, R.E., Sherman, A.D., Robison, B.H., 2017. New technology reveals the role of giant larvaceans in oceanic carbon cycling. Sci. Adv. 3, e1602374.

Kelley, D., Richards, C., Layton, C., 2018. Package 'oce.'.

Lampitt, R.S., Salter, I., de Cuevas, B.A., Hartman, S., Larkin, K.E., Pebody, C.A., 2010. Long-term variability of downward particle flux in the deep northeast Atlantic: causes and trends. Deep-Sea Res. Part II 57, 1346–1361.

Last, K.S., Hobbs, L., Berge, J., Brierley, A.S., Cottier, F., 2016. Moonlight drives ocean-scale mass vertical migration of zooplankton during the Arctic winter. Curr. Biol. 26, 244–251.

Lauerman, L.M.L., Kaufmann, R.S., Smith Jr., K.L., 1996. Distribution and abundance of epibenthic megafauna at a long time-series station in the abyssal northeast Pacific. Deep-Sea Res. Part I 43, 1075–1103.

Lazaridis, E., 2014. Lunar: Lunar Phase & Distance, Seasons and Other Environmental Factors. R Package version 0.1-04.

Le Moigne, F.A.C., 2019. Pathways of organic carbon downward transport by the oceanic biological carbon pump. Front. Mar. Sci. 6, 634.

Ligges, U., Short, T., Kienzle, P., Schnackenberg, S., Billinghurst, D., Borchers, H.-W., Carezia, A., Dupuis, P., Eaton, J.W., Farhi, E., others, 2015. Package 'signal.' R Found. Stat. Comput..

Liszka, C.M., Manno, C., Stowasser, G., Robinson, C., Tarling, G.A., 2019. Mesozooplankton community composition controls faecal pellet flux and remineralisation depth in the Southern Ocean. Front. Mar. Sci. 6, 230.

Liu, Y., Sun, S., Zhang, G., 2012. Seasonal variation in abundance, diel vertical migration and body size of pelagic tunicate Salpa fusiformis in the Southern Yellow Sea. Chin. J. Oceanol. Limnol. 30, 92–104.

Lundsgaard, C., Olesen, M., 1997. The origin of sedimenting detrital matter in a coastal system. Limnol. Oceanogr. 42, 1001–1005.

Lutz, M.J., Caldeira, K., Dunbar, R.B., Behrenfeld, M.J., 2007. Seasonal rhythms of net primary production and particulate organic carbon flux to depth describe the efficiency of biological pump in the global ocean. J. Geophys. Res. Ocean. 112.

Madin, L.P., 1982. Production, composition and sedimentation of salpfecal pellets in oceanic waters. Mar. Biol. 67, 39–45.

Manno, C., Stowasser, G., Enderlein, P., Fielding, S., Tarling, G.A., 2015. The contribution of zooplankton faecal pellets to deep-carbon transport in the Scotia Sea

(Southern Ocean). Biogeosciences 12, 1955–1965. https://doi.org/10.5194/bg-12-1955-2015.
Matsueda, H., Handa, N., Inoue, I., Takano, H., 1986. Ecological significance of salp fecal pellets collected by sediment traps in the eastern North Pacific. Mar. Biol. 91, 421–431.
McDonnell, A.M.P., Lam, P.J., Lamborg, C.H., Buesseler, K.O., Sanders, R., Riley, J.S., Marsay, C., Smith, H.E.K., Sargent, E.C., Lampitt, R.S., others, 2015. The oceanographic toolbox for the collection of sinking and suspended marine particles. Prog. Oceanogr. 133, 17–31.
McGill, P.R., Henthorn, R.G., Bird, L.E., Huffard, C.L., Klimov, D.V., Smith Jr., K.L., 2016. Sedimentation event sensor: new ocean instrument for in situ imaging and fluorometry of sinking particulate matter. Limnol Oceanogr. Methods 14, 853–863.
McGill, P.R., Sherman, A.D., Hobson, B.W., Henthorn, R.G., Chase, A.C., Smith, K.L., 2007. Initial deployments of the Rover, an autonomous bottom-transecting instrument platform for long-term measurements in deep benthic environments. In: OCEANS 2007, pp. 1–7.
Miquel, J.C., Gasser, B., Martín, J., Marec, C., Babin, M., Fortier, L., Forest, A., 2015. Downward particle flux and carbon export in the Beaufort Sea, Arctic Ocean; the role of zooplankton. Biogeosciences 12, 5103–5117.
Ochoa, J., Maske, H., Sheinbaumc, J., Candela, J., 2013. Diel and lunar cycles of vertical migration extending to below 1000 m in the ocean and the vertical connectivity of depth-tiered populations. Limnol. Oceanogr. 58, 1207–1214.
Ohman, M.D., Romagnan, J.B., 2016. Nonlinear effects of body size and optical attenuation on Diel Vertical Migration by zooplankton. Limnol. Oceanogr. 61, 765–770. https://doi.org/10.1002/lno.10251.
Pascual, M., Acuña, J.L., Sabatés, A., Raya, V., Fuentes, V., 2017. Contrasting diel vertical migration patterns in Salpa fusiformis populations. J. Plankton Res. 39, 836–842.
Purcell, J.E., Madin, L.P., 1991. Diel patterns of migration, feeding, and spawning by salps in the subarctic Pacific. Mar. Ecol. Prog. Ser. 73, 211–217.
R Core Team, 2019. R: A Language and Environment for Statistical Computing. R Foundation for Statistical Computing, Vienna, Austria, ISBN 3-900051-07-0 (URL).
Ransom, B., Shea, K.F., Burkett, P.J., Bennett, R.H., Baerwald, R., 1998. Comparison of pelagic and nepheloid layer marine snow: implications for carbon cycling. Mar. Geol. 150, 39–50.
Reigstad, M., Riser, C.W., Svensen, C., 2005. Fate of copepod faecal pellets and the role of Oithona spp. Mar. Ecol.: Prog. Ser. 304, 265–270.
Riley, J.S., Sanders, R., Marsay, C., Le Moigne, F.A.C., Achterberg, E.P., Poulton, A.J., 2012. The relative contribution of fast and slow sinking particles to ocean carbon export. Global Biogeochem. Cycles 26.
Robison, B.H., Bailey, T.G., 1981. Sinking rates and dissolution of midwater fish fecal matter. Mar. Biol. 65, 135–142.
Robison, B.H., Reisenbichler, K.R., Sherlock, R.E., 2005. Giant larvacean houses: rapid carbon transport to the deep sea floor. Science 308, 1609–1611.
Ruhl, H.A., 2008. Community change in the variable resource habitat of the abyssal northeast Pacific. Ecology 89, 991–1000.
Ruhl, H.A., Bahr, F.L., Henson, S.A., Hosking, W.B., Espinolac, B., Kahru, M., Daniela, P., Drake, P., Edwards, C.A., 2020. Understanding the remote influences of ocean weather on the episodic pulses of particulate organic carbon flux. Deep-Sea Res. Part II. This volume.
Saba, G.K., Steinberg, D.K., 2012. Abundance, composition, and sinking rates of fish fecal pellets in the Santa Barbara Channel. Sci. Rep. 2, 716.
Sakuma, K.M., Field, J.C., Mantua, N.J., Ralston, S., Marinovic, B.B., Carrion, C.N., 2016. Anomalous epipelagic micronekton assemblage patterns in the neritic waters of the California Current in spring 2015 during a period of extreme ocean conditions. CALCOFI (Calif. Coop. Ocean. Fish. Investig.) Rep. 57, 163–183.
Sasikumar, G., Ragesh, N., Sajikumar, K.K., Koya, K.P., Durgekar, R.N., Joseph, M., Alloycious, P.S., Kripa, V., Mohamed, K.S., 2014. Zooplankton phototaxis in oceanic squid fishing grounds in the Arabian Sea. Indian J. Geo-Mar. Sci. 43 (8), 1528–1532.
Schindelin, J., Arganda-Carreras, I., Frise, E., Kaynig, V., Longair, M., Pietzsch, T., Preibisch, S., Rueden, C., Saalfeld, S., Schmid, B., others, 2012. Fiji: an open-source platform for biological-image analysis. Nat. Methods 9, 676.
Schlining, B.M., Stout, N.J., 2006. MBARI's video annotation and reference system. In: Proceedings of the Marine Technology Society/Institute of Electrical and Electronics Engineers Oceans Conference, pp. 1–5.
Shatova, O., Koweek, D., Conte, M.H., Weber, J.C., 2012. Contribution of zooplankton fecal pellets to deep ocean particle flux in the Sargasso Sea assessed using quantitative image analysis. J. Plankton Res. 34, 905–921.
Sherman, A.D., Smith Jr., K.L., 2009. Deep-sea benthic boundary layer communities and food supply: a long-term monitoring strategy. Deep-Sea Res. Part II 56, 1754–1762.
Silver, M.W., 1975. The habitat of Salpa fusiformis in the California Current as defined by indicator assemblages 1. Limnol. Oceanogr. 20, 230–237.
Silver, M.W., Gowing, M.M., 1991. The "particle" flux: origins and biological components. Prog. Oceanogr. 26, 75–113.
Smith Jr., K.L., 1987. Food energy supply and demand: a discrepancy between particulate organic carbon flux and sediment community oxygen consumption in the deep ocean 1. Limnol. Oceanogr. 32, 201–220.
Smith Jr., K.L., Baldwin, R.J., Glatts, R.C., Kaufmann, R.S., Fisher, E.C., 1998. Detrital aggregates on the sea floor: chemical composition and aerobic decomposition rates at a time-series station in the abyssal NE Pacific. Deep-Sea Res. Part II 45, 843–880.
Smith Jr., K.L., Druffel, E.R.M., 1998. Long time-series monitoring of an abyssal site in the NE Pacific: an introduction. Deep-Sea Res. Part II 45, 573–586.
Smith Jr., K.L., Glatts, R.C., Baldwin, R.J., Beaulieu, S.E., Uhlman, A.H., Horn, R.C., Reimers, C.E., 1997. An autonomous. bottom-transecting vehicle for making long time-series measurements of sediment community oxygen consumption to abyssal depths. Limnol. Oceanogr. 42, 1601–1612.
Smith Jr., K.L., Huffard, C.L., McGill, P.R., Sherman, A.D., Connolly, T.P., Von Thun, S., Kuhnz, L.A., 2020. Gelatinous zooplankton abundance and benthic boundary layer currents in the abyssal Northeast Pacific: a 3-yr time series study. Deep-Sea Res. Part II Top. Stud. Oceanogr. 104654 this volume.
Smith, K.L., Huffard, C.L., Sherman, A.D., Ruhl, H.A., 2016. Decadal change in sediment community oxygen consumption in the abyssal northeast Pacific. Aquat. Geochem. 22, 401–417.
Smith Jr., K.L., Kaufmann, R.S., Wakefield, W.W., 1993. Mobile megafaunal activity monitored with a time-lapse camera in the abyssal North Pacific. Deep-Sea Res. Part I 40, 2307–2324.
Smith, K.L., Laver, M.B., 1981. Respiration of the bathypelagic fish Cyclothone acclinidens. Mar. Biol. 61, 261–266.
Smith, K.L., Ruhl, H.A., Bett, B.J., Billett, D.S.M., Lampitt, R.S., Kaufmann, R.S., 2009. Climate, carbon cycling, and deep-ocean ecosystems. Proc. Natl. Acad. Sci. U.S.A. 106, 19211–19218.
Smith Jr., K.L., Ruhl, H.A., Huffard, C.L., Messie, M., Kahru, M., 2018. Episodic organic carbon fluxes from surface ocean to abyssal depths during long-term monitoring in NE Pacific. Proc. Natl. Acad. Sci. U.S.A. 115, 12235–12240.
Smith, K.L., Ruhl, H.A., Kahru, M., Huffard, C.L., Sherman, A.D., 2013. Deep ocean communities impacted by changing climate over 24 y in the abyssal northeast Pacific Ocean. Proc. Natl. Acad. Sci. 110, 19838–19841.
Smith Jr., K.L., Sherman, A.D., Huffard, C.L., McGill, P.R., Henthorn, R., Von Thun, S., Ruhl, H.A., Kahru, M., Ohman, M.D., 2014. Large salp bloom export from the upper ocean and benthic community response in the abyssal northeast Pacific: day to week resolution. Limnol. Oceanogr. 59, 745–757.
Smith Jr., K.L., Sherman, A.D., McGill, P.R., Henthorn, R.G., Ferreira, J., Huffard, C.L., 2017. Evolution of monitoring an abyssal time- series station in the northeast Pacific over 28 years. Oceanography 30 (4), 72–81. https://doi.org/10.5670/oceanog.2017.425.
Soetaert, K., Soetaert, M.K., 2016. Package 'OceanView'.
Steinberg, D.K., Carlson, C.A., Bates, N.R., Johnson, R.J., Michaels, A.F., Knap, A.H., 2001. Overview of the US JGOFS Bermuda Atlantic Time-series Study (BATS): a decade-scale look at ocean biology and biogeochemistry. Deep-Sea Res. Part II 48 (8–9), 1405–1447.
Stone, J.P., Steinberg, D.K., 2014. Long-term time-series study of salp population dynamics in the Sargasso Sea. Mar. Ecol. Prog. Ser. 510, 111–127.
Strickland, J.D.H., Parsons, T.R., 1972. A Practical Handbook of Seawater Analysis. Fisheries Research Board of Canada, Ottawa.
Stukel, M.R., Aluwihare, L.I., Barbeau, K.A., Chekalyuk, A.M., Goericke, R., Miller, A.J., Ohman, M.D., Ruacho, A., Song, H., Stephens, B.M., others, 2017. Mesoscale ocean fronts enhance carbon export due to gravitational sinking and subduction. Proc. Natl. Acad. Sci. 114, 1252–1257.
Svensen, C., Riser, C.W., Reigstad, M., Seuthe, L., 2012. Degradation of copepod faecal pellets in the upper layer: role of microbial community and Calanus finmarchicus. Mar. Ecol. Prog. Ser. 462, 39–49.
Thiel, H., Pfannkuche, O., Schriever, G., Lochte, K., Gooday, A.J., Hemleben, C., Mantoura, R.F.G., Turley, C.M., Patching, J.W., Riemann, F., 1989. Phytodetritus on the deep-sea floor in a central oceanic region of the Northeast Atlantic. Biol. Oceanogr. 6, 203–239.
Turner, J.T., 2015. Zooplankton fecal pellets, marine snow, phytodetritus and the ocean's biological pump. Prog. Oceanogr. 130, 205–248.
Turnewitsch, R., Dale, A., Lahajnar, N., Lampitt, R.S., Sakamoto, K., 2017. Can neap-spring tidal cycles modulate biogeochemical fluxes in the abyssal near-seafloor water column? Prog. Oceanogr. 154, 1–24.
Turnewitsch, R., Dumont, M., Kiriakoulakis, K., Legg, S., Mohn, C., Peine, F., Wolff, G., 2016. Tidal influence on particulate organic carbon export fluxes around a tall seamount. Prog. Oceanogr. 149, 189–213.
Urban-Rich, J., Hansell, D.A., Roman, M.R., 1998. Analysis of copepod fecal pellet carbon using a high temperature combustion method. Mar. Ecol.: Prog. Ser. 171, 199–208.
Urrere, M.A., Knauer, G.A., 1981. Zooplankton fecal pellet fluxes and vertical transport of particulate organic material in the pelagic environment. J. Plankton Res. 3, 369–388.
van der Walt, S., Schönberger, J.L., Nunez-Iglesias, J., Boulogne, F., Warner, J.D., Yager, N., Gouillart, E., Yu, T., scikit-image contributors, 2014. scikit- image: image processing in Python. PeerJ 2, e453.
Vangriesheim, A., Springer, B., Crassous, P., 2001. Temporal variability of near-bottom particle resuspension and dynamics at the Porcupine abyssal plain, northeast atlantic. Prog. Oceanogr. 50, 123–145.
Vinogradov, Evgen'evich, Mikhail, 1970. Vertical Distribution of the Oceanic Zooplankton, vol. 1. Israel Program for Scientific Translations [available from the US Department of Commerce Clearinghouse for Federal Scientific and Technical Information, Springfield, Va.].
Wakefield, W.W., Genin, A., 1987. The use of a Canadian (perspective) grid in deep-seaphotography. Deep-Sea Res. Part A. Oceanogr. Res. Pap. 34, 469–478.
Walsh, I., Fischer, K., Murray, D., Dymond, J., 1988. Evidence for resuspension of rebound particles from near-bottom sediment traps. Deep-Sea Res. Part A 35, 59–70.
Watanabe, H., Moku, M., Kawaguchi, K., Ishimaru, K., Ohno, A., 1999. Diel vertical migration of myctophid fishes (Family Myctophidae) in the transitional waters of the western North Pacific. Fish. Oceanogr. 8, 115–127.
Wickham, H., Wickham, M.H., 2007. The Ggplot Package.
Wiebe, P.H., Madin, L.P., Haury, L.R., Harbison, G.R., Philbin, L.M., 1979. Diel vertical migration by *Salpa aspera* and its potential for large-scale particulate organic matter transport to the deep-sea. Mar. Biol. 53, 249–255.

Wigham, B.D., Hudson, I.R., Billett, D.S.M., Wolff, G.A., 2003. Is long-term change in the abyssal Northeast Atlantic driven by qualitative changes in export flux? Evidence from selective feeding in deep-sea holothurians. Prog. Oceanogr. 59, 409–441.
Wilson, S.E., Ruhl, H., Smith Jr., K.L., 2013. Zooplankton fecal pellet flux in the abyssal northeast Pacific: a 15 year time-series study. Limnol. Oceanogr. 58, 881–892.
Wilson, S.E., Steinberg, D.K., Buesseler, K.O., 2008. Changes in fecal pellet characteristics with depth as indicators of zooplankton repackaging ofparticles in the mesopelagic zone of the subtropical and subarctic NorthPacific Ocean. Deep-Sea Res. Part II 55, 1636–1647.
Witbaard, R., Duineveld, G.C.A., Van der Weele, J.A., Berghuis, E.M., Reyss, J.L., 2000. The benthic response to seasonal deposition of phytodetritus at the Porcupine abyssal plain in the North east atlantic. J. Sea Res. 43, 15–31.
Witte, U., Wenzhofer, F., Sommer, S., Boetius, A., Heinz, P., Aberle, N., Sand, M., Cremer, A., Abraham, W.-R., Jorgensen, B.B., Pfannkuche, O., 2003. In situ experimental evidence of the fate of a phytodetritus pulse at the abyssal sea floor. Nature 424, 763–766.
Wong, C.S., Whitney, F.A., Crawford, D.W., Iseki, K., Matear, R.J., Johnson, W.K., Page, J.S., Timothy, D., 1999. Seasonal and interannual variability in particle fluxes of carbon, nitrogen, and silicon, from time series traps at Ocean Station P, 1982–1993: relationships to changes in subarctic primary productivity. Deep-Sea Res. Part II 46, 2735–2760.
Wood, S.N., 2011. Fast stable restricted maximum likelihood and marginal likelihood estimation of semiparametric generalized linear models. J. R. Stat. Soc. Ser. B 1, 3–36.
Yentsch, C.S., Phinney, D.A., 1985. Spectral fluorescence: an ataxonomic tool for studying the structure of phytoplankton populations. J. Plankton Res. 7, 617–632.